Hall effect and resistivity in high-T_c superconductors: The conserving approximation

Hiroshi Kontani
Institute for Solid State Physics, University of Tokyo, 7-22-1 Roppongi, Minato-ku, Tokyo 106-8666, Japan

Kazuki Kanki
College of Integrated Arts and Sciences, Osaka Prefecture University, Sakai 599-8531, Japan

Kazuo Ueda
Institute for Solid State Physics, University of Tokyo, 7-22-1 Roppongi, Minato-ku, Tokyo 106-8666, Japan

(Received 15 October 1998)

The Hall coefficient R_H in high-T_c cuprates in the normal state shows the striking non-Fermi-liquid behavior: R_H follows a Curie-Weiss type temperature dependence and $|R_H| \gg 1/|ne|$ at low temperatures in the underdoped compounds. Moreover, R_H is positive for hole-doped compounds and negative for electron-doped ones, although each of them has a similar holelike Fermi surface. In this paper, we give the explanation of this long-standing problem from the standpoint of the nearly antiferromagnetic (AF) Fermi liquid. We consider seriously the vertex corrections for the current which are indispensable to satisfy the conservation laws, which are violated within the conventional Boltzmann transport approximation. The obtained total current $\vec{J}_{\mathbf{k}}$ takes an enhanced value and is no longer perpendicular to the Fermi surface due to the strong AF fluctuations. By virtue of this mechanism, the anomalous behaviors of R_H in high-T_c cuprates are naturally explained. Both the temperature and the (electron, hole) doping dependences of R_H in high-T_c cuprates are reproduced well by numerical calculations based on the fluctuation-exchange approximation, applied to the single-band Hubbard model with a holelike Fermi surface. We also discuss the singular temperature dependence of R_H in other nearly AF metals, e.g., V_2O_3, κ-BEDT-TTF organic superconductors, and heavy fermion systems close to the AF phase boundary. [S0163-1829(99)13321-6]

I. INTRODUCTION

In the normal state of high-T_c superconductors (HTSC's), various quantities deviate from the conventional Fermi-liquid behaviors.[1] These non-Fermi-liquid features have been studied intensively both theoretically and experimentally because they have close relation to the mechanism of high-T_c superconductivity. For example, the electrical resistivity ρ and the longitudinal NMR relaxation rate $1/T_1$ in HTSC's show universally the behaviors $\rho \propto T$, $1/T_1 \propto T^0$ for a wide range of temperatures.[2] These are quite different from the conventional Fermi-liquid behaviors, $\rho \propto T^2$, $1/T_1 \propto T$.

In HTSC's, the Hall coefficient R_H also shows an interesting non-Fermi-liquid behavior: It shows a drastic temperature dependence although the Fermi surfaces (FS's) in HTSC's are nondegenerate and simple in shape. At high temperatures ($\sim$1000 K), R_H takes a nearly constant value, and its doping dependence is very small. Its value is close to the one estimated by the LDA band calculation $R_H^{\rm band}$.[3] And the doping dependence of R_H is also very small there.

On the other hand, as the temperature decreases, R_H begins to show a Curie-Weiss type temperature dependence, and its maximum value is a few times larger than $R_H^{\rm band}$ at the optimum doping. This enhancement of R_H further increases in the underdoped region. In the hole-doped compounds, e.g., $YBa_2Cu_3O_{7-\delta}$ (YBCO) or $La_{2-\delta}Sr_\delta CuO_4$ (LSCO), $dR_H/dT<0$ is observed and R_H is positive for a wide range of temperatures.[4–9] On the other hand, in the electron-doped compounds, e.g., $Nd_{2-\delta}Ce_\delta CuO_4$ (NCCO), $dR_H/dT>0$ is realized and the sign of R_H changes to negative at low temperature although its FS is holelike.[4,10,11] Figure 1 shows a summary of experimental results of LSCO and NCCO in the underdoped region, where an approximate electron-hole symmetry is realized.[4] In both compounds, $|R_H|$ increases near half filling.

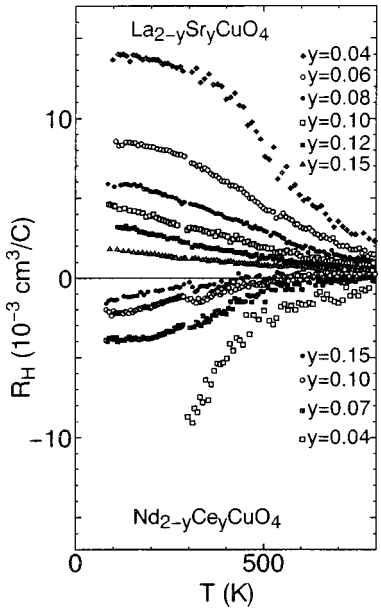

FIG. 1. Temperature dependence of R_H in LSCO (hole doping) and NCCO (electron doping) in the paramagnetic state. Note that $1/|ne| \sim 1.5\times 10^{-3}$ cm^3 C in HTSC's.

The Hall effect is one of the unsolved problems in HTSC's. Its unusual features mentioned above are summarized as follows. (i) The Curie-Weiss type behavior of R_H in a quite wide range of temperatures. (ii) The enhancement of R_H in the underdoped region. (iii) $R_H<0$ in the electron-doped compounds.

Nowadays, various non-Fermi-liquid phenomena of HTSC have been explained by using different types of spin-fluctuation theories, e.g., the SCR theory,[12] the spin-fluctuation model,[13] and the fluctuation-exchange (FLEX) theory.[14,15] They can explain a reasonable T_c of the $d_{x^2-y^2}$ superconductivity. They can also explain the pseudogap formation in density of states,[16–18] the shadow band formation,[16] and the collective modes emerging below T_c.[19,20]

So far, various attempts have been made on the Hall effect in HTSC's.[21–24] Some of them are in the framework of the spin fluctuation model, by using the Boltzmann transport approximation (or one-loop approximation).[23,24] However, the Boltzmann approximation cannot explain the magnitude of $|R_H|$ in the underdoped region. Moreover, it predicts $R_H>0$ for both YBCO and NCCO because they have similar holelike FS's. This result contradicts with the experiments, shown in Fig. 1. Therefore, the behavior of R_H noted as (i)–(iii) above have cast some suspicion on the validity of the nearly antiferromagnetic (AF) Fermi liquid description for HTSC.

In this paper, we study the Hall effect of HTSC's based on a conserving approximation.[25,26] We use the expressions for the conductivity (σ_{xx}) and the Hall conductivity (σ_{xy}/H) derived from the Kubo formula.[27–30] Then, we study the total current $\vec{J}_{\mathbf{k}}$ including all the vertex corrections so that the conservation laws are satsfied (i.e., conserving approximation). We find that $\vec{J}_{\mathbf{k}}$ shows critical behaviors which are a natural consequence of the strong backward scatterings by the AF fluctuations. By virtue of this fact, the present theory succeeds in explaining the overall features of R_H, noted as (i)–(iii) above, without assuming a non-Fermi liquid ground state. We also find that the conventional Boltzmann approximation, where the conservation laws are violated, cannot reproduce any of (i)–(iii).

We analyze the extended Hubbard model as an effective model for HTSC's. We use the FLEX approximation to calculate the Green function and the self-energy.[14,15] It is a kind of self-consistent perturbation theory with respect to U, and it has advantages for handling large spin fluctuations.

Phenomenologically, the spin propagator in HTSC's is expressed for small $\mathbf{q}$ and ω as follows:[12,13,23]

$$\chi^s_{\mathbf{q}}(\omega)=\frac{\chi_Q}{1+\xi^2(\mathbf{q}-\mathbf{Q})^2+\mathrm{i}\omega/\omega_{\mathrm{sf}}}, \tag{1}$$

where $\mathbf{Q}$ is the AF wave vector, and ξ is the AF correlation length. Experimentally, ξ^2 follows a Curie-Weiss type temperature dependence below $\sim$1000 K in many HTSC's. It ceases to increase at T_c in the overdoped region, or at the characteristic temperature $T^*(>T_c)$ in the underdoped region. We call T^* the pseudo-spin-gap temperature as usual. In general, the following relations are satisfied for $T>T^*$ experimentally:[31]

$$\xi^2\approx\alpha_0/(T+\Theta), \tag{2}$$

$$\chi_Q\approx\alpha_1\xi^2, \quad 1/\omega_{\mathrm{sf}}\approx\alpha_2\xi^2, \tag{3}$$

where Θ, α_0, α_1, and α_2 are constants.[32] The coefficient α_0 increases rapidly in the underdoped region, and ξ^2 reaches $\sim O(100)$ at T^* nearby the half filling (we put the unit-cell length $a=1$) and α_2 decreases rather moderately in the underdoped region. The relation $\omega_{\mathrm{sf}}\gtrsim T$ ($\omega_{\mathrm{sf}}\lesssim T$) is satisfied in the overdoped (underdoped) region.

The typical spin-fluctuation theories reproduce the experimental relations (2) and (3) for $T>T^*$.[18] Moreover, the following relations are obtained by the spin-fluctuation theories:[12,23,24,33]

$$\rho\propto CT^2, \quad 1/T_1\propto CT, \tag{4}$$

where C has a strong temperature dependence in the nearly AF Fermi liquid. According to them, $C\propto\xi^2\propto 1/T$ is derived, so the experimentally observed non-Fermi-liquid behaviors of ρ and $1/T_1$ are explained well by the spin-fluctuation theories. One may naturally expect that the T dependence of R_H is also governed by the spin fluctuations. In this paper, we find that $R_H\propto\xi^2$ through the vertex corrections for the current. A similar study based on the phenomenological AF spin-fluctuation model is reported in another paper.[34]

The contents of this paper are as follows. In Sec. II, we introduce the single-band Hubbard model with some sets of parameters corresponding to YBCO, LSCO, and NCCO. In Sec. III, we review the general formulation for σ_{xx} and σ_{xy}/H based on the Fermi-liquid theory, and rewrite σ_{xy}/H into a simpler form. In Sec. IV, the vertex corrections to the current is studied by using the conserving approximation. We find that only the Maki-Thompson term is dominant. In Sec. V, we solve the Bethe-Salpeter equation for the total current $\vec{J}_{\mathbf{k}}$ analytically, and derive the relation $R_H\propto\xi^2$. In Sec. VI, numerical results for ρ and R_H obtained by the FLEX theory are presented, which are consistent with the experimental behaviors in HTSC's. Finally, in Sec. VII, the Hall effect in heavy fermion systems is discussed briefly. The readers who are mainly interested in the numercal calculation of R_H can proceed to Sec. VI B for the first reading, where the sufficient set of equations for the numerical calculations for σ_{xx} and σ_{xy}/H are explained shortly.

II. MODEL HAMILTONIAN

In this paper, we treat the following extended Hubbard model with (U,t_0,t_1,t_2):

$$H=\sum_{\mathbf{k}\sigma}\epsilon^0_{\mathbf{k}}c^\dagger_{\mathbf{k}\sigma}c_{\mathbf{k}\sigma}+U\sum_{\mathbf{k}\mathbf{k}'\mathbf{q}}c^\dagger_{\mathbf{k}+\mathbf{q}\uparrow}c^\dagger_{\mathbf{k}'-\mathbf{q}\downarrow}c_{\mathbf{k}'\downarrow}c_{\mathbf{k}\uparrow}, \tag{5}$$

$$\epsilon^0_{\mathbf{k}}=2t_0[\cos(k_x)+\cos(k_y)]+4t_1\cos(k_x)\cos(k_y)+2t_2[\cos(2k_x)+\cos(2k_y)], \tag{6}$$

where $c^\dagger_{\mathbf{k}\sigma}$ is the creation operator of an electron with momentum $\mathbf{k}$ and spin σ, and U is the on-site Coulomb repulsion. We represent the filling of the electrons by n, and $n=1$ corresponds to the half filling.

Taking the results by the LDA band calculation into account,[35–38] we choose the following set of parameters. (I)

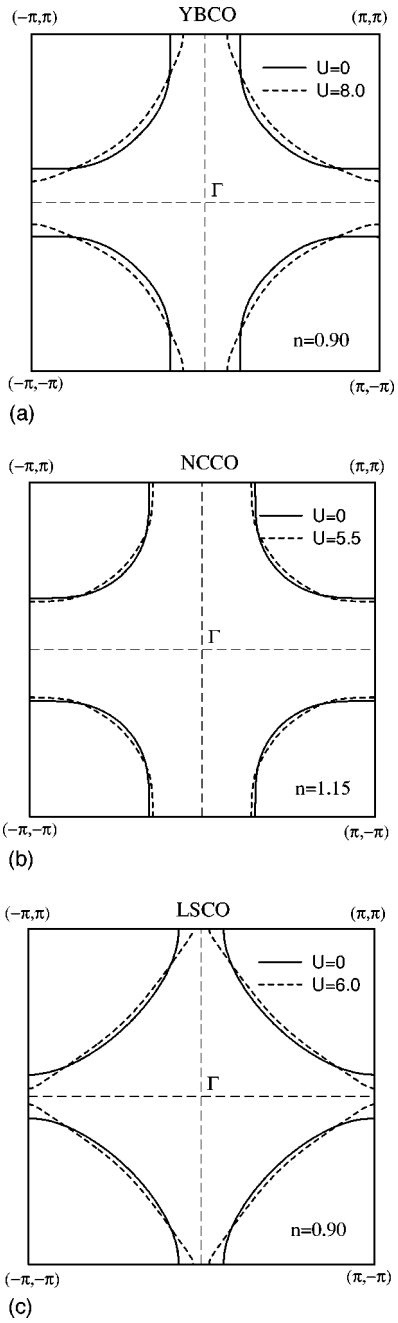

FIG. 2. Fermi surface of (a)YBCO, (b)NCCO, and (c)LSCO. In (a) and (b), $t_0=-1$, $t_1=1/6$, and $t_2=-1/5$. In (c), $t_0=-1$, $t_1=1/10$, and $t_2=-1/10$.

YBCO (hole doping), NCCO (electron doping): $t_0=-1$, $t_1=1/6$, $t_2=-1/5$.[35,36,39] (II) LSCO (hole-doping): $t_0=-1$, $t_1=1/10$, $t_2=-1/10$.[37,38] Figure 2 shows the Fermi surfaces (FS's) for $U=0$, together with those for finite U calculated by the FLEX approximation at $T=0.02$. In the case of (I), the FS is holelike everywhere and the spectrum at $(\pi,0)$ is below the chemical potential μ at least for $n>0.6$. On the other hand, in the case of (II) the spectrum at $(\pi,0)$ is above μ for $n<0.77$ at $U=0$, and $n\lesssim 0.85$ for $U=6$, respectively. These characters of the calculated FS's coincide qualitatively with those by the LDA band calculations[35–38] or by the angle resolved photoemission (ARPES) experiments.[40–42]

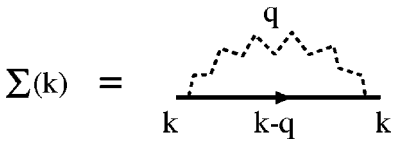

FIG. 3. The self-energy of the FLEX theory. The full line and the wavy line represent $G(k-q)$ and $V(q)$, respectively.

Here, we summarize the formalism of the FLEX theory which will be used throughout this paper. The Dyson equation is written as

$$\{G_{\mathbf{k}}(\epsilon_n)\}^{-1}=i\epsilon_n+\mu-\epsilon^0_{\mathbf{k}}-\Sigma_{\mathbf{k}}(\epsilon_n), \tag{7}$$

The self-energy is given by

$$\Sigma_{\mathbf{k}}(\epsilon_n)=T\sum_{\mathbf{q},l} G_{\mathbf{k}-\mathbf{q}}(\epsilon_n-\omega_l)V_{\mathbf{q}}(\omega_l), \tag{8}$$

$$V_{\mathbf{q}}(\omega_l)=U^2\left(\frac{3}{2}\chi^s_{\mathbf{q}}(\omega_l)+\frac{1}{2}\chi^c_{\mathbf{q}}(\omega_l)-\chi^0_{\mathbf{q}}(\omega_l)\right)+U, \tag{9}$$

$$\chi^s_{\mathbf{q}}(\omega_l)=\chi^0_{\mathbf{q}}\{1-U\chi^0_{\mathbf{q}}(\omega_l)\}^{-1}, \tag{10}$$

$$\chi^c_{\mathbf{q}}(\omega_l)=\chi^0_{\mathbf{q}}\{1+U\chi^0_{\mathbf{q}}(\omega_l)\}^{-1}, \tag{11}$$

$$\chi^0_{\mathbf{q}}(\omega_l)=-T\sum_{\mathbf{k},n} G_{\mathbf{q}+\mathbf{k}}(\omega_l+\epsilon_n)G_{\mathbf{k}}(\epsilon_n), \tag{12}$$

where $\epsilon_n=(2n+1)\pi T$ and $\omega_l=2l\pi T$, respectively. The self-energy is shown by Fig. 3. We solve Eqs. (7)–(12) self-consistently, choosing the chemical potential μ so as to keep the filling constant $n=T\Sigma_{\mathbf{k},n}G_{\mathbf{k}}(\epsilon_n)e^{-i\epsilon_n 0}$.

In a Fermi liquid, the real-frequency Green function in the vicinity of $\omega\sim 0$ and $|\mathbf{k}|\sim k_{\mathrm{F}}$ is represented as

$$G_{\mathbf{k}}(\omega)=z_{\mathbf{k}}/(\omega+\mu-\epsilon_{\mathbf{k}}-\mathrm{i}z_{\mathbf{k}}\Delta_{\mathbf{k}}), \tag{13}$$

where $z_{\mathbf{k}}$ is the renormalization factor given by $z_{\mathbf{k}}=[1-\partial\Sigma_{\mathbf{k}}(\omega)/\partial\omega]^{-1}$, $\epsilon_{\mathbf{k}}$ is the quasiparticle spectrum given by the solution of $\mathrm{Re}\{G_{\mathbf{k}}(\omega)\}^{-1}=0$, and $\Delta_{\mathbf{k}}=-\mathrm{Im}\,\Sigma_{\mathbf{k}}(\omega+i\delta)>0$. The density of states (DOS) is given by

$$\rho_{\mathbf{k}}(\omega)=-\frac{1}{\pi}\mathrm{Im}\,G_{\mathbf{k}}(\omega+\mathrm{i}\delta). \tag{14}$$

In the case of $z_{\mathbf{k}}\Delta_{\mathbf{k}}\ll T$, $\rho_{\mathbf{k}}(\omega)=z_{\mathbf{k}}\delta(\omega+\mu-\epsilon_{\mathbf{k}})$.

The FLEX approximation is suitable for the analysis of the nearly AF Fermi liquid. It has been applied to the square lattice Hubbard model by many authors.[14,16–18,20,49] Though it is an approximation, imaginary time Green function obtained by the FLEX agrees with the results by the QMC simulation very well for a moderate U.[14] Recently, it has also been applied to the superconducting ladder compound $Sr_{14-x}Ca_xCu_{24}O_{41}$ (Ref. 43) and the organic superconducting κ-BEDT-TTF compounds.[44,45]

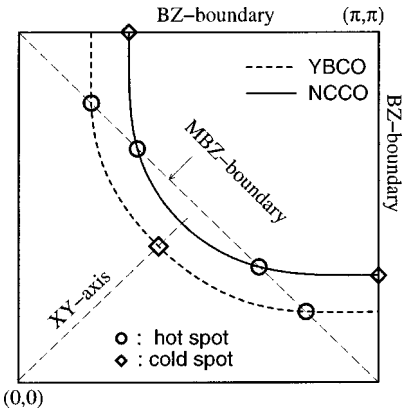

FIG. 4. The hot spots and the cold spots in YBCO and NCCO, respectively.

Here, we comment on the change of the FS. Figure 2 shows that the shape of the FS changes as a function of $U>0$. It also means that the FS changes significantly depending on the temperature. The effect of this change on R_H is discussed in Sec. VI. We also comment on the anisotropy of $\Delta_{\mathbf{k}}$ on the FS, which becomes larger as the AF fluctuation grows at low temperatures. $\Delta_{\mathbf{k}}$ takes a large value around the crossing points with the magnetic Brillouin zone (MBZ) boundary, which we call hot spots as often referred to in the literature.[23,24] $\Delta_{\mathbf{k}}$ becomes small at the points where the distance from the MBZ boundary is the largest, which are called cold spots. (see Fig. 4). These cold spots play major role for ρ and R_H. We study this subject in Sec. VI in detail.

Finally, we discuss on the validity and the limitation of the FLEX theory on HTSC's. In the FLEX approximation, Eqs. (2) and (3) are satisfied well, and the coefficient α_0 in Eq. (2) increases rapidly as n approaches to the half filling ($n=1$). Moreover, the relation $\omega_{\rm sf}\lesssim T$ ($w_{\rm sf}\gtrsim$T) in the underdoped (overdoped) region is satisfied qualitatively as shown in Table I, which is consistent with experiments. However, the FLEX approximation cannot explain the experimentally observed pseudo-spin-gap behaviors for $T^*>T>T_c$, where ξ cease to increase and $1/\omega_{\rm sf}$ begins to decrease as the temperature decreases. It would also be inapplicable near the Mott-insulating state, i.e., $0.9\gtrsim n\gtrsim 1.1$. In this paper we perform numerical studies for $n\leqslant 0.9$ or $n\geqslant 1.1$, where the FLEX approximation gives reasonable results.

III. FORMALISM OF CONDUCTIVITY IN THE FERMI LIQUID THEORY

In this section, we review the transport theory. By the Kubo formula, the conductivity is given by

$$\sigma_{\mu\nu}=e^2\sum_{\mathbf{k}\mathbf{k}'\sigma\sigma'} v^0_{\mathbf{k}\mu}v^0_{\mathbf{k}'\nu}\frac{\mathrm{Im}\,K_{\mathbf{k}\sigma,\mathbf{k}'\sigma'}(\omega+i\delta)}{\omega}\bigg|_{\omega=0}, \quad (15)$$

TABLE I. The value of $\omega_{\rm sf}$ for $n=0.90$ (underdoped), $n=0.85$ (nearly optimum), and $n=0.80$ (overdoped) obtained by the FLEX approximation at $T=0.02$.

	$n=0.90$	$n=0.85$	$n=0.80$
YBCO ($U=8$)	0.018	0.034	0.046
LSCO ($U=6$)	0.013	0.019	0.024

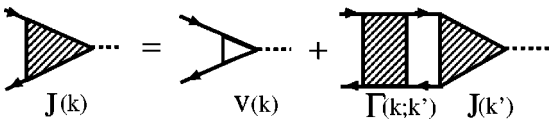

FIG. 5. The BS equation for $J_{\mathbf{k}\mu}$.

$$K_{\mathbf{k}\sigma,\mathbf{k}'\sigma'}(i\omega_n)=\int_0^{1/T} d\tau\, e^{\omega_n\tau}\langle T_\tau\{c^\dagger_{\mathbf{k}\sigma}(\tau)c_{\mathbf{k}\sigma}(\tau)c^\dagger_{\mathbf{k}'\sigma'}c_{\mathbf{k}'\sigma'}\}\rangle, \quad (16)$$

where $v^0_{\mathbf{k}\mu}(k)=\partial\epsilon^0_{\mathbf{k}}/\partial k_\mu$ and $\omega_n=2\pi Tn$ is the even Matsubara frequency, and $e(>0)$ is the absolute value of the charge of an electron. In the absence of the magnetic field, the analytic continuation from $K_{\mathbf{k}\sigma,\mathbf{k}'\sigma'}(i\omega_n)$ to $K_{\mathbf{k}\sigma,\mathbf{k}'\sigma'}(\omega+i\delta)$ has been performed by Eliashberg.[27] According to him, the conductivity carried by the quasiparticles are given by

$$\sigma_{xx}=e^2\sum_{\mathbf{k}}\left(-\frac{\partial f}{\partial\epsilon}\right)_{\epsilon_{\mathbf{k}}} z_{\mathbf{k}}v_{\mathbf{k}x}J_{\mathbf{k}x}\frac{1}{\Delta_{\mathbf{k}}}, \quad (17)$$

where $f(\epsilon)=1/(1+e^{(\epsilon-\mu)/T})$. In Eq. (17) we have done the energy integration by assuming the relation $z_{\mathbf{k}}\Delta_{\mathbf{k}}\ll T$, which is not always satisfied in HTSC's as shown in Sec. VI, however.

In Eq. (17), $v_{\mathbf{k}x}$ and $J_{\mathbf{k}x}$ are given by

$$v_{\mathbf{k}x}=\frac{\partial}{\partial k_x}[\,\epsilon^0_{\mathbf{k}}+\mathrm{Re}\,\Sigma_{\mathbf{k}}(\omega=0)\,], \quad (18)$$

$$J_{\mathbf{k}x}=v_{\mathbf{k}x}+\sum_{\mathbf{k}'}\int_{-\infty}^{\infty}\frac{d\epsilon}{4\pi i}\mathcal{T}_{\mathbf{k}\mathbf{k}'}(0,\epsilon)|G_{\mathbf{k}'}(\epsilon)|^2J_{\mathbf{k}'x}, \quad (19)$$

where $\mathcal{T}_{\mathbf{k}\mathbf{k}'}(\epsilon,\epsilon')$ is the irreducible four point vertex introduced by Eliashberg, which is discussed in the next section in detail. It plays an important role to treat the umklapp processes of conduction electrons.[28] The total current $\vec{J}_{\mathbf{k}}$ is given by the solution of the Bethe-Salpeter (BS) equation (19), which is shown by Fig. 5.

The Hall coefficient R_H under a weak magnetic field along z axis H is give by

$$R_H=\frac{\sigma_{xy}/H}{\sigma_{xx}\sigma_{yy}}. \quad (20)$$

The analytic continuation for the normal Hall conductivity σ_{xy} due to the quasiparticle contribution in the presence of the magnetic field H has been performed by Kohno and Yamada,[29] or Fukuyama *et al.*,[30] in the gauge invariant manner. According to them, assuming that the fourfold symmetry of the system

$$\sigma_{\mu\nu}/H=-\epsilon_{\mu\nu z}\frac{1}{2}e^3\sum_{\mathbf{k}}\left(-\frac{\partial f}{\partial\epsilon}\right)_{\epsilon_{\mathbf{k}}} A_{\mu\nu}(\mathbf{k})\frac{z_{\mathbf{k}}}{(\Delta_{\mathbf{k}})^2},$$

$$A_{\mu\nu}(\mathbf{k})=v_{\mathbf{k}\mu}\left[J_{\mathbf{k}\mu}\frac{\partial J_{\mathbf{k}\nu}}{\partial k_\nu}-J_{\mathbf{k}\nu}\frac{\partial J_{\mathbf{k}\mu}}{\partial k_\nu}\right], \quad (21)$$

where $\epsilon_{xyz}=-\epsilon_{yxz}=1$, reflecting Onsagaer's reciprocity theorem. Equation (21) means $\sigma_{xy}/H\propto(\Delta_{\mathbf{k}})^{-2}$, whereas

$\sigma_{xx} \propto (\Delta_{\mathbf{k}})^{-1}$ by Eq. (17). Thus, R_H = const in the conventional Fermi liquid at low temperatures.

The expression (21) can be rewritten into a simpler form, where there is only the symmetry with respect to the origin [see Eq. (3.21) of Ref. 29]

$$\sigma_{xy}/H = -\frac{e^3}{4}\sum_k \left(-\frac{\partial f}{\partial \epsilon}\right)_{\epsilon_{\mathbf{k}}} A_s(\mathbf{k})\frac{z_{\mathbf{k}}}{(\Delta_{\mathbf{k}})^2},$$

$$\begin{aligned} A_s(\mathbf{k}) &= A_{xy}(\mathbf{k}) + A_{yx}(\mathbf{k}) \\ &= [J_{\mathbf{k}x}(\vec{e}_z \times \vec{v}_{\mathbf{k}})\vec{\nabla}\cdot J_{\mathbf{k}y} - \langle x \leftrightarrow y \rangle] \\ &= |\vec{v}_{\mathbf{k}}|\left(\vec{J}_{\mathbf{k}} \times \frac{\partial}{\partial k_\parallel}\vec{J}_{\mathbf{k}}\right)_z \\ &= |\vec{v}_{\mathbf{k}}| \cdot |\vec{J}_{\mathbf{k}}|^2 \left(\frac{d\theta_J(\mathbf{k})}{dk_\parallel}\right), \end{aligned} \tag{22}$$

where $k_\parallel$ is the component of $\vec{k}$ along the vector $\vec{e}_\parallel(\mathbf{k}) = (\vec{e}_z \times \vec{v}_{\mathbf{k}})/|\vec{v}_{\mathbf{k}}|$, and tangential to the FS at $\mathbf{k}$ because $\vec{v}_{\mathbf{k}}$ is perpendicular to the FS. In Eq. (22), $\theta_J(\mathbf{k})$ is the angle between $\vec{J}_{\mathbf{k}}$ and the x axis except for an arbitrary constant. Contrary to $A_{\mu\nu}(\mathbf{k})$, $A_s(\mathbf{k})$ introduced in Eq. (22) is a scalar variable, i.e., independent of the choice of coordinates. As a result, we know that σ_{xy}/H is also independent of the choice of coordinates, if only the reflection symmetry exists. This property of σ_{xy}/H has been proved so far only by the Boltzmann transport theory.[46–48]

By using the relation $d\epsilon_{\mathbf{k}}/dk_\mu = z_{\mathbf{k}} v_{\mathbf{k}\mu}$, Eq. (22) becomes

$$\sigma_{xy}/H = -\frac{e^3}{4}\oint_{\mathrm{FS}} dk_\parallel |\vec{J}_{\mathbf{k}}|^2 \left(\frac{d\theta_J(\mathbf{k})}{dk_\parallel}\right)\frac{1}{(\Delta_{\mathbf{k}})^2} \tag{23}$$

at sufficiently low temperatures. In this line integration, the $\mathbf{k}$ point moves anticlockwise along the FS.

Finally, we discuss the Boltzmann transport approximation. The conductivity in the magnetic field $\vec{H}$ is given by $\sigma_{\mu\nu} = e\Sigma_{\mathbf{k}}(-\partial f/\partial \epsilon_{\mathbf{k}}) v_{\mathbf{k}\mu}\Phi_\nu(\vec{v}_{\mathbf{k}})$ for $\vec{E} \| \vec{e}_\nu$, where $\Phi_\nu(\vec{v}_{\mathbf{k}}) = [1 - e\Delta_{\mathbf{k}}^{-1}(\vec{v}_{\mathbf{k}} \times \vec{H})\cdot\vec{\nabla}]\cdot(e\Delta_{\mathbf{k}}^{-1} v_{\mathbf{k}\nu})$ up to the first order of $\vec{H}$ within the relaxation time approximation.[47] As a result, the conductivity in this approximation σ^0_{xx} is given by Eq. (17) by replacing $\vec{J}_{\mathbf{k}}$ with $\vec{v}_{\mathbf{k}}$. In the same way, the Hall conductivity within the relaxation time approximation σ^0_{xy} is given by

$$\sigma^0_{xy}/H = -\frac{e^3}{4}\oint_{\mathrm{FS}} dk_\parallel |\vec{v}_{\mathbf{k}}|^2 \left(\frac{d\theta_v(\mathbf{k})}{dk_\parallel}\right)\frac{1}{(\Delta_{\mathbf{k}})^2}, \tag{24}$$

where $\theta_v(\mathbf{k})$ is the angle between $\vec{v}_{\mathbf{k}}$ and the x axis. Thus, the sign of σ^0_{xy}/H is determined by the sign of $[d\theta_v(\mathbf{k})/dk_\parallel]$, which is nothing but the curvature of the FS at $\mathbf{k}$.[46–48]

In the later sections, we calculate $J_{\mathbf{k}\mu}$ by solving Eq. (19). In the nearly AF Fermi liquid, we find that $\vec{J}_{\mathbf{k}}$ is no longer perpendicular to the FS, so $[d\theta_J(k)/dk_\parallel]$ and $[d\theta_v(k)/dk_\parallel]$ at the same $\mathbf{k}$ can be quite different, even in sign. This is the reason why the Boltzmann approximation fails to reproduce the anomalous behavior of R_H in HTSC.

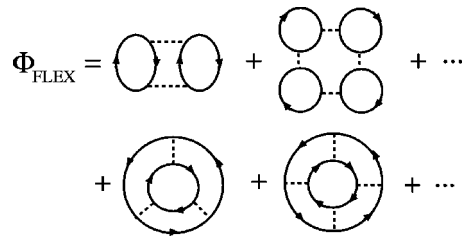

FIG. 6. Each full line represents the dressed Green function $G_{\mathbf{k}}(\omega)$ and each broken line represents U.

IV. VERTEX CORRECTIONS FROM $\mathcal{T}_{\mathbf{k},\mathbf{k}'}(\epsilon,\epsilon')$

In this section, we study the vertex corrections for the current, which is essential for the transport phenomena. The self-energy in the FLEX theory, which is given by Eq. (8), is also obtained by the functional derivative of Φ_{FLEX} as $\Sigma_{\mathbf{k}}(\epsilon) = \delta\Phi_{\mathrm{FLEX}}/\delta G_{\mathbf{k}}(\epsilon)$, where Φ_{FLEX} is given by the closed skeleton diagrams made of $G_{\mathbf{k}}(\epsilon)$ and U, with a factor $1/n$ for U^n diagrams. The existence of Φ_{FLEX}, which is depicted in Fig. 6, means that the FLEX theory is classified as a conserving approximation whose framework was constructed by Baym and Kadanoff[25] and Baym.[26] In the conserving approximation, the particle-hole transport function L is given as the solution of the BS equation, where the irreducible particle-hole vertex $\Gamma_{\mathbf{k}\mathbf{k}'}(\epsilon,\epsilon') = \delta\Sigma_{\mathbf{k}}(\epsilon)/\delta G_{\mathbf{k}'}(\epsilon')$ is used as the kernel. Then, the L obtained in this way satisfies various conservation laws automatically. This is the reason why we call it the conserving approximation.

Significance of the conserving approximation in the calculation of correlation functions is well recognized in various situations. Conductivity is one typical quantity. Within the conserving approximation, Yamada and Yosida show that the conductivity given by Eq. (17) diverges at finite temperatures in the absence of the umklapp processes, reflecting the momentum conservation law. Their work shows that the vertex correction from $\mathcal{T}_{\mathbf{k}\mathbf{k}'}(\epsilon,\epsilon')$ in Eq. (19), which is neglected within the Boltzmann theory, is necessary to treat the momentum dissipation through the umklapp scattering processes of electrons.

The irreducible particle-hole vertex $\Gamma_{\mathbf{k}\mathbf{k}'}(\epsilon,\epsilon')$ within the FLEX theory is shown in Fig. 7:

$$\Gamma_{\mathbf{k}\mathbf{k}'}(\epsilon_n,\epsilon_{n'};\omega_l) = \Gamma^{(a)} + \Gamma^{(b)} + \Gamma^{(c)}, \tag{25}$$

where $\omega_l = 2l\pi T$ is the external frequency, and $\epsilon_n = (2n+1)\pi T$ is the odd Matsubara frequency. We put the external momentum zero. $\Gamma^{(a)}$-$\Gamma^{(c)}$ are given by

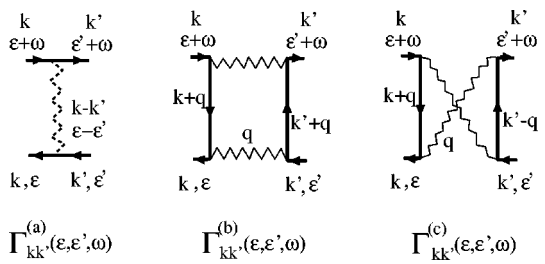

FIG. 7. The irreducible four-point vertexes, which are sufficient for the conserving approximation. In (a), the wavy line represents $V(k-k')$. In (b) and (c), the two wavy lines represent $W(q)$ and the q summation should be taken.

$$\Gamma^{(a)}_{\mathbf{k}\mathbf{k}'}(\epsilon_n,\epsilon_{n'};\omega_l)=V_{\mathbf{k}-\mathbf{k}'}(\epsilon_n-\epsilon_{n'}), \tag{26}$$

$$\Gamma^{(b)}_{\mathbf{k}\mathbf{k}'}(\epsilon_n,\epsilon_{n'};\omega_l)=-T\sum_{\mathbf{q},l'} W_{\mathbf{q}}(\omega_{l'},\omega_{l'}-\omega_l) \times G_{\mathbf{k}+\mathbf{q}}(\epsilon_n+\omega_{l'})G_{\mathbf{k}'+\mathbf{q}}(\epsilon_{n'}+\omega_{l'}), \tag{27}$$

$$\Gamma^{(c)}_{\mathbf{k}\mathbf{k}'}(\epsilon_n,\epsilon_{n'};\omega_l)=-T\sum_{\mathbf{q},l'} W_{\mathbf{q}}(\omega_{l'},\omega_{l'}+\omega_l) \times G_{\mathbf{k}+\mathbf{q}}(\epsilon_n+\omega_{l'}+\omega_l)G_{\mathbf{k}'-\mathbf{q}}(\epsilon_{n'}-\omega_{l'}), \tag{28}$$

where $V_{\mathbf{k}}(\epsilon_n)$ is given by Eq. (9), and we have introduced $W_{\mathbf{k}}(\omega_l,\omega_{l'})$ as

$$W_{\mathbf{k}}(\omega_l,\omega_{l'})=\frac{3}{2}U^2[U\chi^s_{\mathbf{k}}(\omega_l)+1][U\chi^s_{\mathbf{k}}(\omega_{l'})+1] +\frac{1}{2}U^2[U\chi^c_{\mathbf{k}}(\omega_l)-1][U\chi^c_{\mathbf{k}}(\omega_{l'})-1]-U^2. \tag{29}$$

These three irreducible vertices $\Gamma^{(a)}$, $\Gamma^{(b)}$ and $\Gamma^{(c)}$ are sufficient for the conserving approximation. In the literature, process (a) is called the Maki-Thompson (MT) term, and (b) and (c) are called Aslamazov-Larkin (AL) terms.

In order to solve the BS equation (19), we have to obtain the functional form of the irreducible vertex $\mathcal{T}_{\mathbf{k}\mathbf{k}'}(\epsilon,\epsilon')$ in Eq. (19). For this purpose, we perform the analytic continuation of $\Gamma^{(a)}$, $\Gamma^{(b)}$, and $\Gamma^{(c)}$ with respect to ϵ_n and $\epsilon_{n'}$ in Appendix A. We note that $\mathcal{T}_{\mathbf{k}\mathbf{k}'}(\epsilon,\epsilon')$ is nothing but the $\mathcal{T}^{(0)}_{22}(\epsilon,\epsilon')$ in Eliashberg's paper.[27] This correction gives rise to singular temperature dependence of the Hall coefficient in HTSC's (see Sec. V).

Now, we obtain the vertex corrections for the current by replacing $\mathcal{T}_{\mathbf{k}\mathbf{k}'}(0,\epsilon)$ in Eq. (19) with $\mathcal{T}^{(a-c)}_{\mathbf{k}\mathbf{k}'}(0,\epsilon)$ given by Eqs. (A9)–(A11). At first, the contribution coming from $\mathcal{T}^{(a)}_{\mathbf{k}\mathbf{k}'}$ is given by

$$\Delta J^a_{\mathbf{k}\mu}=\frac{1}{2}\sum_{\mathbf{k}'}\int d\epsilon'\left(\mathrm{cotanh}\frac{\epsilon'}{2T}-\tanh\frac{\epsilon'}{2T}\right) \times \mathrm{Im}\,V_{\mathbf{k}'-\mathbf{k}}(\epsilon'+i\delta)\rho_{\mathbf{k}'}(\epsilon')\frac{1}{\Delta_{\mathbf{k}'}(\epsilon')}J_{\mathbf{k}'\mu}, \tag{30}$$

where we put $\epsilon=0$, and we have used the relation $|G_{\mathbf{k}}(\epsilon)|^2=\pi\rho_{\mathbf{k}}(\epsilon)/\Delta_{\mathbf{k}}(\epsilon)$. These vertex corrections play an important role in the singular behavior of the Hall coefficient. in HTSC's, which will be discussed in Sec. V.

Next, we consider the correction terms coming from $\mathcal{T}^{(b)}_{\mathbf{k}\mathbf{k}'}$ and $\mathcal{T}^{(c)}_{\mathbf{k}\mathbf{k}'}$. Approximately, they are given by

$$\Delta J^{b,c}_{\mathbf{k}\mu}=\frac{\pi}{4}\sum_{\mathbf{k}'}\int d\epsilon\left(\mathrm{cotanh}\frac{\epsilon}{2T}-\tanh\frac{\epsilon}{2T}\right)\sum_{\mathbf{q}}\int d\omega\, W_{\mathbf{q}}(\omega) \times\left(\tanh\frac{\omega+\epsilon}{2T}-\tanh\frac{\omega}{2T}\right)\rho_{\mathbf{k}+\mathbf{q}}(0)\rho_{\mathbf{k}'+\mathbf{q}}(0) \times\frac{\rho_{\mathbf{k}'}(0)}{\Delta_{\mathbf{k}'}(0)}J_{\mathbf{k}'\mu}, \tag{31}$$

where $W_{\mathbf{q}}(\omega)$ is introduced by Eq. (A6). Here we have neglected the ω dependences of $\rho_{\mathbf{k}}(\omega)$ and $\Delta_{\mathbf{k}}(\omega)$ because only the regions $|\omega|,|\epsilon|\lesssim\min\{T,\omega_{\mathrm{sf}}\}$ are important in the ω,ϵ integrations in Eq. (31). The variable change $\mathbf{k}'\to-\mathbf{k}'$ is performed for $\Delta\vec{J}^c_{\mathbf{k}}$. Thus, $\Delta\vec{J}^b_{\mathbf{k}}$ and $\Delta\vec{J}^c_{\mathbf{k}}$ are equal in this approximation, which is not a rigorous relation, however.

Now, we show that Eq. (31) is negligible in the case of $\xi^2\gg1$ and $\mathbf{Q}=(\pi,\pi)$. In this case, the leading contributions in the $\mathbf{q}$ summation in Eq. (31) come only from $\mathbf{q}\sim\mathbf{Q}$. In the $\mathbf{k}'$ summation of Eq. (31), there is a cancellation between the contributions from $\mathbf{k}'$ and $-\mathbf{k}'$ if we put $\mathbf{q}=\mathbf{Q}$, because $\mathbf{k}'+\mathbf{Q}$ and $\mathbf{k}'-\mathbf{Q}$ are the same in the momentum space. As a result, we expect that both $\Delta J^b_{\mathbf{k}\mu}$ and $\Delta J^c_{\mathbf{k}\mu}$ are negligibly smaller than $\Delta J^a_{\mathbf{k}\mu}$. This statement becomes rigorous in the case of $\xi^2\to\infty$. In Appendix B, we show this cancellation in the two AL terms explicitly by the numerical calculations. This is one of the main conclusions of this paper.

V. ANALYSIS FOR THE BETHE-SALPETER (BS) EQUATION FOR $J_{\mathbf{k}\mu}$

The aim of this section is to give the qualitative understanding of the mechanism for the temperature dependence of R_H in HTSC's. We try an analytical approach to solve the BS equation (19) for $J_{\mathbf{k}\mu}$, by neglecting the AL terms. To simplify the discussion, we assume that $\mathbf{Q}=(\pi,\pi)$, where the MBZ boundary is defined by the line between $(\pi,0)$ and $(0,\pi)$. This situation is realized in YBCO experimentally.

For a qualitative discussion, we use the phenomenological expression for $\chi^s_{\mathbf{q}}(\omega)$ given by Eq. (1) and neglect other terms in the definition of $V_{\mathbf{q}}(\omega)$ in Eq. (9). We introduce the function $H(x)=1/x-2\psi(x+1)+2\psi(x+\frac{1}{2})$, where $\psi(x)$ is the digamma function. Then, the imaginary part of the self-energy is given by

$$\Delta_{\mathbf{k}}=\sum_{\mathbf{q}}\int\frac{d\epsilon}{2\pi}\left[\mathrm{cotanh}\frac{\epsilon}{2T}-\tanh\frac{\epsilon}{2T}\right] \times\pi\rho_{\mathbf{k}-\mathbf{q}}(\epsilon)\,\mathrm{Im}\,V_{\mathbf{q}}(\epsilon+i\delta) =\frac{3U^2}{4}\sum_{\mathbf{q}}\chi_Q\omega_{\mathrm{sf}}H\left(\frac{\omega_{\mathbf{q}}}{2\pi T}\right)\rho_{\mathbf{k}-\mathbf{q}}(0), \tag{32}$$

$$H\left(\frac{\omega_{\mathbf{q}}}{2\pi T}\right)\approx\frac{(\pi T)^2}{\omega_{\mathbf{q}}(\omega_{\mathbf{q}}+\pi T/2)}, \tag{33}$$

where $\omega_{\mathbf{q}}=\omega_{\mathrm{sf}}+\omega_{\mathrm{sf}}\xi^2(\mathbf{q}-\mathbf{Q})^2$.[23,24] The approximate form of $H(\omega_{\mathbf{q}}/2\pi T)$ given by Eq. (33) becomes exact both for $\omega_{\mathrm{sf}}\gg T$ and $\omega_{\mathrm{sf}}\ll T$. Here, the average of Δ_k over the FS is given by

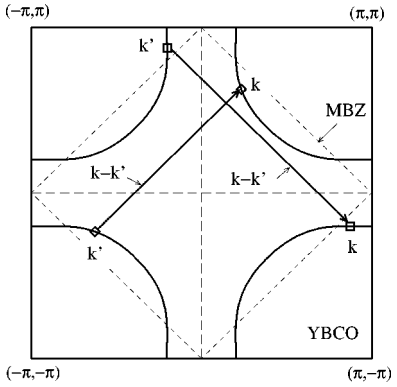

FIG. 8. The relation between $\mathbf{k}$ and $\mathbf{k}'$. Both points locate on the FS.

$$\langle \Delta_{\mathbf{k}} \rangle_{\mathrm{FS}} \equiv \sum_{\mathbf{k}} \Delta_{\mathbf{k}} \rho_{\mathbf{k}}(0)$$

$$= \frac{3U^2}{4} \sum_{\mathbf{q}} \frac{\chi_Q \omega_{\mathrm{sf}} (\pi T)^2}{\omega_{\mathbf{q}} (\omega_{\mathbf{q}} + \pi T/2)} \left. \frac{\partial \, \mathrm{Im} \, \chi^0_{\mathbf{q}}(\omega + i\delta)}{\partial \omega} \right|_{\omega=0}$$

$$\propto \chi_Q T \xi^{-2} [1 - (1 + \pi T / 2\omega_{\mathrm{sf}})^{-1/2}], \tag{34}$$

where we have assumed that the $\mathbf{q}$ dependence of $(\partial/\partial\omega)\mathrm{Im}\,\chi^0_{\mathbf{q}}(\omega + i\delta)|_{\omega=0}$ is moderate. As a result,

$$\langle \Delta_{\mathbf{k}} \rangle_{\mathrm{FS}} \propto \begin{cases} \xi^2 T^2 \propto T & \text{for } \omega_{\mathrm{sf}} \gtrsim T, \\ \xi^0 T \propto T & \text{for } \omega_{\mathrm{sf}} \lesssim T, \end{cases} \tag{35}$$

which is independent of ξ for $\omega_{\mathrm{sf}} \lesssim T$ (underdoped region). Because the resistivity ρ is approximately proportional to $\langle \Delta_{\mathbf{k}} \rangle_{\mathrm{FS}}$, $\rho \propto T$ is expected for various filling n, which is consistent with experiments. We calculate ρ more exactly in Sec. VI B.

Next, we examine the vertex correction for the current, which is given by Eq. (30). We stress that $\mathrm{Im}\, V_{\mathbf{k}}(\omega)$ appearing in Eqs. (30) and (32) are the same, which is ensured in the conserving approximation. We can show that

$$\Delta J_{\mathbf{k}\mu} = \frac{3U^2}{4} \sum_{\mathbf{q}} \chi_Q \omega_{\mathrm{sf}} H\left(\frac{\omega_{\mathbf{q}}}{2\pi T} \right) \frac{\rho_{\mathbf{k}-\mathbf{q}}(0)}{\Delta_{\mathbf{k}-\mathbf{q}}} J_{\mathbf{k}-\mathbf{q}\mu}. \tag{36}$$

Comparing Eq. (36) with Eq. (32), and noticing that $H(\omega_{\mathbf{q}} 2\pi T)$ is negligibly small for $|\mathbf{Q} - \mathbf{q}| \gtrsim \xi^{-1}$, we get

$$\Delta \vec{J}_{\mathbf{k}} \approx \langle \ \vec{J}_{\mathbf{q}} \ \rangle_{|\mathbf{q}-\mathbf{k}'|<1/\xi}$$

$$\approx \vec{J}_{\mathbf{k}'} \langle \cos[\theta_J(\mathbf{q}) - \theta_J(\mathbf{k}')] \rangle_{|\mathbf{q}-\mathbf{k}'|<1/\xi}, \tag{37}$$

where $\mathbf{k}$, $\mathbf{k}'$, and $\mathbf{q}$ are on the FS. Here, we have introduced $\mathbf{k}'$ so that $\mathbf{k}'$ and $\mathbf{k}$ have the relation $(k'_x, k'_y) = (-k_y, -k_x)$ for $k_x k_y > 0$ and $(k'_x, k'_y) = (k_y, k_x)$ for $k_x k_y < 0$, respectively. The positions of $\mathbf{k}$ and $\mathbf{k}'$ are shown in Fig. 8. We see that $\mathbf{k}' \approx \mathbf{k} + \mathbf{Q}$ is satisfied in the momentum space. Moreover, we assume $|\mathbf{Q} - (\mathbf{k} - \mathbf{k}')| \lesssim \xi^{-1}$ everywhere on the FS because it seems to be satisfied in the present numerical calculation by the FLEX approximation. Thus, we obtain a simplified BS equation

$$\vec{J}_{\mathbf{k}} = \vec{v}_{\mathbf{k}} + \alpha_{\mathbf{k}} \cdot \vec{J}_{\mathbf{k}'}, \tag{38}$$

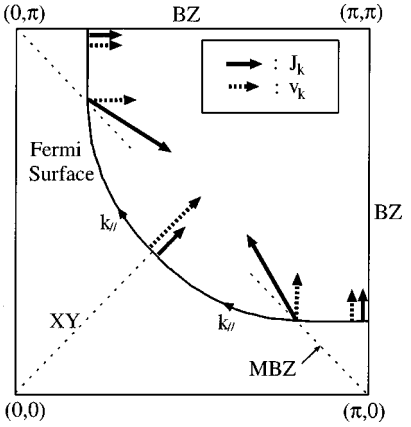

FIG. 9. Schematic behaviors of $\vec{J}_{\mathbf{k}}$ and $\vec{v}_{\mathbf{k}}$. Contrary to $\vec{v}_{\mathbf{k}}$, $\vec{J}_{\mathbf{k}}$ is not perpendicular to the FS. For example, $(d\theta_J/dk_{\|}) < 0$ on the XY line, and $(d\theta_J/dk_{\|}) > 0$ on the BZ boundary [see Eq. (39)].

where $\alpha_{\mathbf{k}} \approx (1 - c/\xi^2) < 1$ and $c \sim O(1)$ is a constant. $\alpha_{\mathbf{k}}$ takes the maximum value around the hot spots.

Now, Eq. (38) can be easily solved as

$$\vec{J}_{\mathbf{k}} = \frac{1}{1 - \alpha^2_{\mathbf{k}}} (\vec{v}_{\mathbf{k}} + \alpha_{\mathbf{k}} \vec{v}_{\mathbf{k}'}). \tag{39}$$

Equation (39) means that $\vec{J}_{\mathbf{k}}$ is not parallel to $\vec{v}_{\mathbf{k}}$. For example, (i) at $k_x = k_y$, $\vec{J}_{\mathbf{k}} = \vec{v}_{\mathbf{k}}/(1 + \alpha_{\mathbf{k}}) \sim \frac{1}{2} \vec{v}_{\mathbf{k}}$ is satisfied. (ii) Near the MBZ boundary, $\vec{J}_{\mathbf{k}} \approx (\xi^2/2c)(\vec{v}_{\mathbf{k}} + \vec{v}_{\mathbf{k}'})$, which is nearly parallel or perpendicular to $\mathbf{Q}$. (iii) On the BZ boundary, $\vec{J}_{\mathbf{k}} \| \vec{v}_{\mathbf{k}}$ because of the symmetry. Moreover, $\vec{J}_{\mathbf{k}} \approx \vec{v}_{\mathbf{k}}$ since the contribution from $\mathbf{k}'$ point cancels out with that from $-\mathbf{k}'$ point approximately, due to the fact that $|\mathbf{k} - \mathbf{k}'| = |\mathbf{k} + \mathbf{k}'| \approx |\mathbf{Q}|$ in the momentum space. Thus, we should put $\alpha_{\mathbf{k}} = 0$ in Eq. (39) on the BZ boundary. These behaviors of $\vec{J}_{\mathbf{k}}$ together with $\vec{v}_{\mathbf{k}}$ are shown schematically in Fig. 9. Physically, this peculiar behavior of $\vec{J}_{\mathbf{k}}$ comes from the multiple backward scattering between $\mathbf{k}$ and $\mathbf{k}'$ caused by the AF fluctuations. Now we stress the importance of the conservation approximation to get the correct $\alpha_{\mathbf{k}}$. For instance, we get $\alpha_{\mathbf{k}} = \infty$ in Eq. (38), if we replace $|G_{\mathbf{k}}(\epsilon)|^2$ with $|G^0_{\mathbf{k}}(\epsilon)|^2$ in Eq. (19), which leads to the divergence of $\vec{J}_{\mathbf{k}}$.

First, we consider the conductivity σ_{xx} by using Eq. (39). According to Eq. (17), σ_{xx} is given by the averaged value of $v_{\mathbf{k}x} \cdot J_{\mathbf{k}x}$ over the FS, that is,

$$v_{\mathbf{k}x} \cdot J_{\mathbf{k}x} = \frac{1}{1 - \alpha^2_{\mathbf{k}}} \{ |v_{\mathbf{k}x}|^2 - \alpha_{\mathbf{k}} | v_{\mathbf{k}x} v_{\mathbf{k}y} | \}. \tag{40}$$

Although $1/(1 - \alpha^2_{\mathbf{k}})$ takes an enhanced value as is discussed above, the resultant σ_{xx} is not enhanced by this factor. For example, if we assume $|v_{\mathbf{k}x}| \approx |v_{\mathbf{k}y}|$, which is satisfied near the cold spots in YBCO and LSCO, then Eq. (40) $\approx |v_{\mathbf{k}x}|^2/(1 + \alpha_{\mathbf{k}})$ is satisfied. This means that the conductivity σ_{xx} is smaller than that given by the Boltzmann approximation, due to the vertex corrections for the current given by $\mathcal{T}_{\mathbf{k}\mathbf{k}'}(\epsilon, \epsilon')$. This is confirmed by the numerical calculations in Sec. VI.

Next, we discuss the Hall conductivity. By using Eq. (39), $dJ_{\mathbf{k}x}/dk_\mu$ is given by

$$\frac{d}{dk_\mu}J_{\mathbf{k}x}=\frac{\mp\beta_{\mathbf{k},\mu}}{1-\alpha_{\mathbf{k}}^2}v_{\mathbf{k}y}+\frac{2\alpha_{\mathbf{k}}\beta_{\mathbf{k},\mu}}{1-\alpha_{\mathbf{k}}^2}J_{\mathbf{k}x}+\frac{1}{1-\alpha_{\mathbf{k}}^2}\left(\frac{dv_{\mathbf{k}x}}{dk_\mu}\mp\alpha_{\mathbf{k}}\frac{dv_{\mathbf{k}y}}{dk_\mu}\right), \tag{41}$$

where $\beta_{\mathbf{k},\mu}\equiv d\alpha_{\mathbf{k}}/dk_\mu$. Hereafter, the $\mp$ in equations is equal to $\mathrm{sgn}(-k_xk_y)$. By using Eq. (36), which gives the definition of $\alpha_{\mathbf{k}}$, then $\beta_{\mathbf{k},\mu}$ is given as

$$\beta_{\mathbf{k},\mu}\approx-\xi^2[\mathbf{Q}-(\mathbf{k}-\mathbf{k}')]_\mu \tag{42}$$

when $|\mathbf{Q}-(\mathbf{k}-\mathbf{k}')|\lesssim\xi^{-1}$ is satisfied. We can see that $\beta_{\mathbf{k},\mu}$ is positive when $\vec{k}+\epsilon\cdot\vec{e}_\mu$ is closer to the MBZ boundary than $\vec{k}$ ($\vec{e}_\mu$ is a unit vector along μ direction, and $\epsilon>0$ is a small constant) and vice versa.

As a result, $A_s(\mathbf{k})$ introduced in Eq. (22) is given by

$$\frac{1}{|\vec{v}_{\mathbf{k}}|}A_s(\mathbf{k})=\frac{1}{1-\alpha_{\mathbf{k}}^2}\left(\vec{v}_{\mathbf{k}}\times\frac{d}{dk_\parallel}\vec{v}_{\mathbf{k}}\right)_z+\frac{\mp\beta_{\mathbf{k},\parallel}}{(1-\alpha_{\mathbf{k}}^2)^2}[v_{\mathbf{k}x}^2-v_{\mathbf{k}y}^2], \tag{43}$$

where we define $k_\parallel$ as the momentum which is tangential to the FS, and is along the anticlockwise direction. Thus, σ_{xy}/H is enhanced by the factor $1/(1-\alpha_{\mathbf{k}}^2)\sim\xi^2/2c$ or $\beta_{\mathbf{k},\parallel}\propto\xi^2$, contrary to the case of σ_{xx}. The first term of Eq. (43) is proportional to the contribution given by the Boltzmann transport theory, whose sign is determined by the curvature of the FS. It takes larger value inside of the MBZ, as shown in Fig. 2. On the other hand, the second term of Eq. (43) is negative inside of the MBZ, and is positive outside of it. Clearly, this term is dominant outside of the MBZ because $|\beta_{\mathbf{k},\parallel}|\gg1$ and $|v_{\mathbf{k}x}^2-v_{\mathbf{k}y}^2|\sim|\vec{v}_{\mathbf{k}}|^2$ is satisfied there. We notice that $\beta_{\mathbf{k},\parallel}=0$ on the MBZ boundary and on the XY axis.

The obtained results in HTSC's are summarized qualitatively as follows (see Fig. 9): The portion of the FS inside of the MBZ gives rise to a positive contribution to R_{H}. In other words, $[d\theta_J(\mathbf{k})/dk_\parallel]<0$ inside of the MBZ. Whereas, the outside part of the MBZ gives rise to a negative contribution to R_{H} in the presence of the strong AF fluctuations because $[d\theta_J(\mathbf{k})/dk_\parallel]>0$ there. In the above $\theta_J(\mathbf{k})$ is introduced in Eq. (23). This change of the sign of R_H never occurs within the Boltzmann approximation because $[d\theta_v(\mathbf{k})/dk_\parallel]<0$ everywhere.

Because of the factor $(\Delta_{\mathbf{k}})^{-2}$ in Eq. (23), the Hall coefficient will be determined by the region near the cold spots. As shown in Fig. 4, the cold spots locate inside (outside) of the MBZ in the case of YBCO (NCCO). As a result, we can understand the reason why $R_H>0$ in the hole doped systems, and why the sign of R_H changes in the electron-doped systems.

In conclusion, the temperature dependence of R_H is proportional to $\xi^2\propto1/T$ both in the hole-doped systems and the electron-doped ones. We find that the T dependence of σ_{xx} and σ_{xy}/H for a system with the strong AF fluctuation are

$$\sigma_{xx}\sim\xi^0/\Delta_{\mathbf{k}},$$

$$\sigma_{xy}/H\sim\pm\xi^2/\Delta_{\mathbf{k}}^2, \tag{44}$$

$$R_H\sim\pm\xi^2\sim\pm\chi_Q,$$

where $+(-)$ is for the hole-doping (electron-doping) case. The factor ξ^2 comes from the vertex corrections for the current introduced in this paper, which does not appear within the Boltzmann approximation. We will confirm the analysis of this section by numerical calculations based on the FLEX theory in the next section.

VI. NUMERICAL RESULTS

A. One-particle properties and magnetic properties obtained by the FLEX approximation

Here, we show electronic properties obtained by the FLEX approximation. They are important to understand the transport quantities. In this section, we use $U=8|t_0|$ for YBCO in numerical calculations, considering that the band width W is $8|t_0|$. On the other hand, we use $U=6|t_0|$ for LSCO and $U=5.5|t_0|$ for NCCO, to reduce the Stoner factor in the FLEX calculation, $\alpha_S=\max_{\mathbf{q}}\{U\chi_{\mathbf{q}}(0)\}$. We have checked the numerical results do not depend on U qualitatively.

In this section, we put $|t_0|=1$. Then, $T=0.1$ will correspond to ~500 K because $|t_0|\sim0.5$ eV in the LDA calculation. In the calculation, 4096 $\mathbf{k}$-point meshes and 256 Matsubara frequencies are used. By solving the linearized Eliashberg equations, we obtain $T_c\approx0.02$ (~100 K) for YBCO and LSCO at $n=0.85$, which is close to the T_c given by the previous works by the FLEX approximation.[15,18,20,49] Also, $T_c\approx0.01$ for NCCO at $n=1.15$. We find that the symmetry of the superconducting state is $d_{x^2-y^2}$-like in all cases.

Figure 10 shows the temperature dependence of the FS's for YBCO, NCCO, and LSCO, respectively. They are determined by the relation $\epsilon_{\mathbf{k}}+\mathrm{Re}\,\Sigma_{\mathbf{k}}(0)=\mu$. In all the cases, the FS's transform so as to strengthen the nesting character as the temperature decreases, which is more prominent in YBCO and LSCO. Apparently, this change of the FS makes $|R_H|$ smaller because its curvature around the cold spots decreases at low temperatures. Now we look at the real part of the self-energy which is the origin of the deformation of the FS. According to Ref. 24,

$$\mathrm{Re}\,\Sigma_{\mathbf{k}}(0)=-\frac{3U^2}{4\pi}\chi_Q\omega_{\mathrm{sf}}\sum_{\mathbf{q}}\frac{1}{\omega_{\mathbf{q}}^2+\epsilon_{\mathbf{k}-\mathbf{q}}^2}\times[2\epsilon_{\mathbf{k}-\mathbf{q}}\ln|\epsilon_{\mathbf{k}-\mathbf{q}}/\omega_{\mathbf{q}}|+\pi\omega_{\mathbf{q}}\,\mathrm{sgn}(\epsilon_{\mathbf{k}-\mathbf{q}})] \tag{45}$$

at $T=0$, where $\epsilon_{\mathbf{k}}$ is measured from μ. This equation means that the sign of $\Sigma_{\mathbf{k}}(0)$ is equal to that of $(\mu-\epsilon_{\mathbf{k}-\mathbf{Q}})$ approximately. This $\mathbf{k}$ dependence of $\Sigma_{\mathbf{k}}(0)$ moves the FS towards the MBZ boundary.

Moreover, in the FLEX approximation, the flat-band structure (i.e., extended saddle point) is created around the van-Hove singularity points $(\pm\pi,0)$ and $(0,\pm\pi)$, because of the renormalization effect by $1/z_{\mathbf{k}}\lesssim10$.[49] This is also the origin of the sensitive temperature dependence of the FS in YBCO and LSCO shown in Fig. 10. This flat-band structure is actually observed by ARPES experiments.[42]

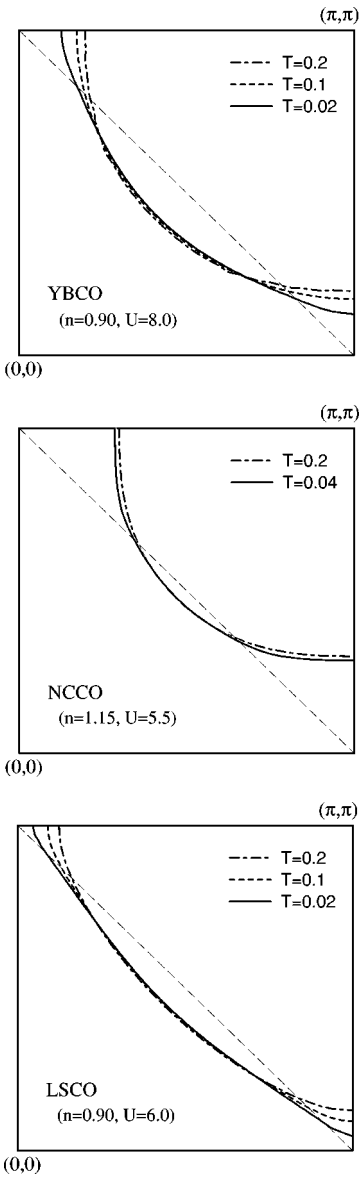

FIG. 10. The temperature dependence of the FS's for various compounds. It is small and negligible in the case of $U=0$.

Next, we consider the **q** dependence of the static magnetic susceptibility $\chi^s_{\mathbf{q}}(0)$, given by Eq. (10). Because it does not contain the vertex corrections required in the conservation approximation, it gives a slightly overestimated value in the underdoped region.[18] In general, the observed $\chi^s_{\mathbf{q}}(0)$ by the neutron diffraction experiments cannot be expressed by the simple phenomenological model, Eq. (1): For YBCO, $\chi^s_{\mathbf{q}}(0)$ shows a peak around $\mathbf{q}\approx\mathbf{Q}=(\pi,\pi)$.[50] On the other hand, it is incommensurate for $La_{2-\delta}Sr_{\delta}CuO_4$, and shows a peak around $\mathbf{q}\approx[(1-\delta)\pi,\pi],[\pi,(1-\delta)\pi]$ for $0.2\gtrsim\delta\gtrsim0.05$.[51]

Figure 11 shows the calculated (q_x,q_y) dependence of $\chi_{\mathbf{q}}(0)$ for YBCO ($n=0.90$, $T=0.02$), NCCO ($n=1.20$, $T=0.02$), and LSCO ($n=0.85$, $T=0.06$), respectively. We see that $\chi_{\mathbf{q}}(0)$ is commensurate for YBCO and NCCO, which is also consistent with neutron diffraction experiments. In the case of LSCO, $\chi_{\mathbf{q}}(0)$ shows an incommensurate structure at low temperatures. At $n=0.85$, the peaks locate at $\mathbf{q}=(0.83\pi,\pi),(\pi,0.83\pi)$ at $T=0.02$, which is consistent with experiments, and it becomes commensurate for

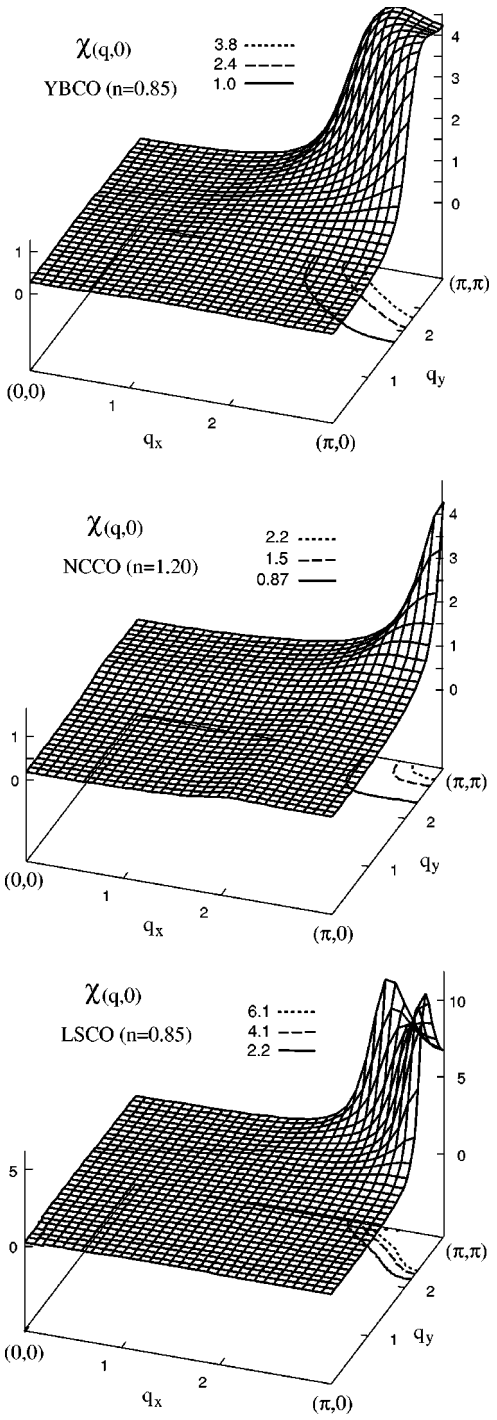

FIG. 11. The (q_x,q_y) dependence of $\chi^s_{\mathbf{q}}(0)$ obtained by the FLEX approximation.

$T\gtrsim0.08$. In conclusion, main characters of $\chi^s_{\mathbf{q}}(0)$ for each compound are reproduced well by the FLEX calculation with appropriate set of parameters $(t_0\sim t_2,U)$.

Figure 12 shows the temperature dependence of $\max_{\mathbf{q}}\{\chi_{\mathbf{q}}(0)\}$ of YBCO, NCCO, and LSCO for different filling numbers. These plots are nothing but the T dependence of ξ^2. Various experimental works on HTSC's by neutron diffraction or by NMR confirm that ξ^2 follows the Curie-Weiss law qualitatively for $T>T^*$, and its Curie constant increases as $n\rightarrow1$.[31,32] As shown in Fig. 12, the FLEX approximation reproduces both the temperature and the doping

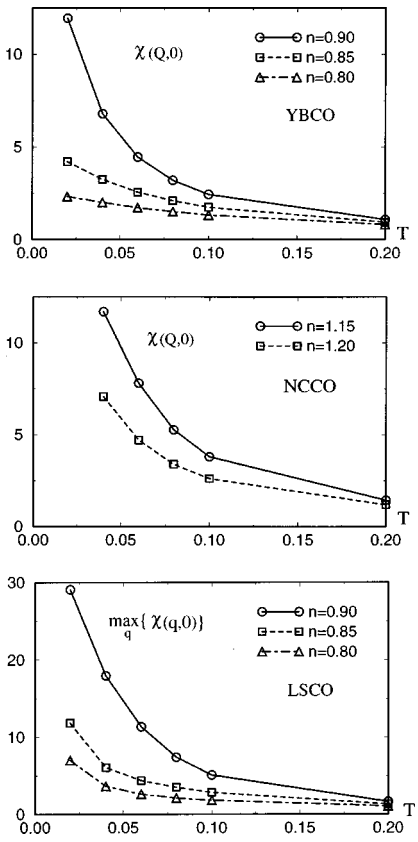

FIG. 12. The temperature dependence of $\max_{\mathbf{q}}\{\chi(\mathbf{q},0)\}$ for various filling numbers. All of them follow the Curie-Weiss law, which is a universal feature of HTSC's. In YBCO and NCCO, $\chi_{\mathbf{q}}(0)$ takes the maximum value at $\mathbf{q}=\mathbf{Q}$. We note that $\chi_{\mathbf{Q}}(0)\propto\xi^2$.

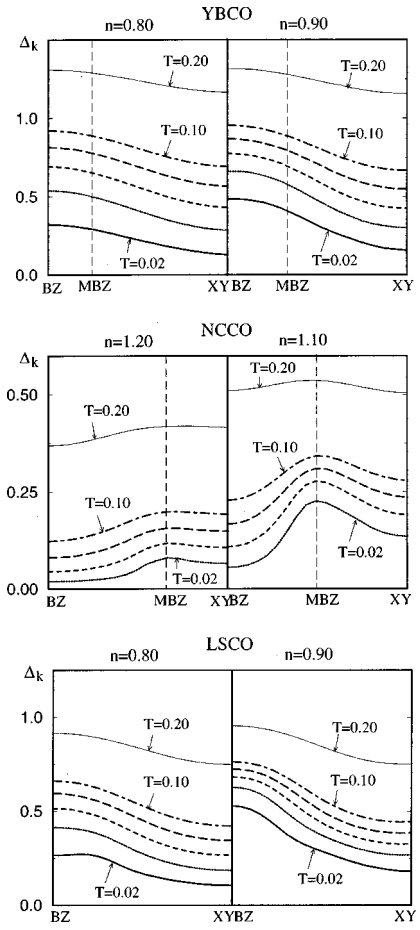

FIG. 13. The $k_{\parallel}$ dependence of $\Delta(k_{\parallel})$ at various temperatures. The T dependence of $\Delta(k_{\parallel})$ at the cold spot and the hot spot are quite different.

dependence of ξ^2 in HTSC's for $T\lesssim 0.1$. However, the calculation of $\chi_{\mathbf{q}}(0)$ including the vertex corrections will be required for more detailed studies.

Finally, we discuss the $\mathbf{k}$ dependence of $\Delta_{\mathbf{k}}=-\mathrm{Im}\,\Sigma_{\mathbf{k}}(0+i\delta)$ on the FS. Here, we define

$$\Delta(k_{\parallel})\equiv\int dk_{\perp}\Delta_{\mathbf{k}}\cdot\rho_{\mathbf{k}}(0)\Big/\int dk_{\perp}\rho_{\mathbf{k}}(0), \qquad (46)$$

where $k_{\parallel}$ and $k_{\perp}$ are the momentum parallel and perpendicular to the FS, respectively. $\Delta(k_{\parallel})$ is an averaged value of $\Delta_{\mathbf{k}}$ over the $k_{\perp}$-direction on the FS, which has a finite width at finite temperatures. Figure 13 shows the $k_{\parallel}$ dependence of $\Delta(k_{\parallel})$ over the 1/8 part of the FS, as shown in Fig. 14. In each case, the relation $z_{\mathbf{k}}\Delta_{\mathbf{k}}\sim T$ is realized around the cold spots because $1/z_{\mathbf{k}}\lesssim 10$ is satisfied.

For YBCO and LSCO, $\Delta(k_{\parallel})$ takes a maximum not on the hot spots shown in Fig. 4, but on the BZ boundary where the flat-band structure is created. As a result, the spectral weight at the Fermi energy is reduced around $(\pi,0)$, which is consistent with ARPES experiments. And $\Delta(k_{\parallel})$ takes a minimum at the cold spot. On the other hand, for NCCO, the hot spot locates close to the XY axis, and the cold spot locates on the BZ boundary. It is quite important that the position of the cold spots changes across $n\approx 1$ by using the FLEX approximation, which causes the change of sign of R_H as shown in Sec. V. To prove this result, the ARPES measurements for NCCO are desired.

As shown in Fig. 13, $\Delta(k_{\parallel})$ at the cold spots decreases in proportion to T qualitatively in all cases, which is consistent with the analysis in Eq. (34). [Note that $\rho_{\mathbf{k}}(0)$ takes larger values around the cold spots.] At the hot spots, however, T dependence of $\Delta(k_{\parallel})$ deviates from T-linear behavior. In fact, $\Delta(k_{\parallel})$ at the hot spot is given by using Eq. (32) as

$$\Delta_{\mathrm{hot}}=\frac{3U^2}{4\pi}\int_{\mathrm{FS}}\frac{dq_{\parallel}}{|v_{\mathbf{q}}|}\chi_Q\omega_{\mathrm{sf}}\frac{(\pi T)^2}{4\omega_{\mathbf{q}}(\omega_{\mathbf{q}}+\pi T/2)}$$
$$\approx\frac{3\pi U^2}{2|v|}\chi_Q T\xi^{-1}[1-(1+\pi T/2\omega_{\mathrm{sf}})^{-1/2}]. \qquad (47)$$

As a result,

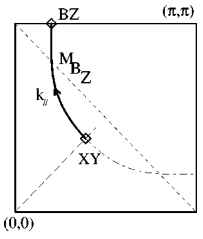

FIG. 14. The path of $k_{\parallel}$ in the case of YBCO.

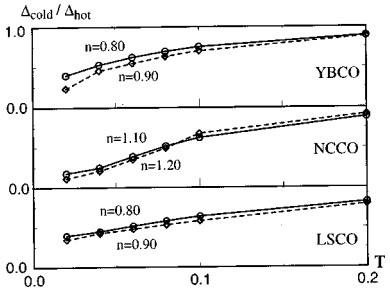

FIG. 15. The temperature dependence of $\Delta_{\rm cold}/\Delta_{\rm hot}$.

$$\Delta_{\rm hot}\propto\begin{cases} T^2\xi^3\propto\sqrt{T} & \text{for } \omega_{\rm sf}\gtrsim T, \\ T\xi\propto\sqrt{T} & \text{for } \omega_{\rm sf}\lesssim T. \end{cases} \tag{48}$$

Thus, we find that $\Delta_{\rm hot}\propto\sqrt{T}$ for a wide range of the filling n, which is clearly seen in Fig. 13 in all the cases. This relation does not contradict with the T-linear resistivity because ρ is determined mainly by the cold spot properties.

Finally, we show the temperature dependence of the anisotropy of $\Delta(k_\parallel)$, $r=\Delta_{\rm cold}/\Delta_{\rm hot}$ in Fig. 15. In all cases, r becomes smaller for the underdoped region, which is consistent with recent ARPES experiments.[52] However, we see that r depends on the shape of the FS sensitively. The relation $r\propto\sqrt{T}$, which is expected according to Eqs. (34) and (47), is satisfield clearly only in YBCO. In conclusion, the relation $r\propto\sqrt{T}$ is less universal than the Curie-Weiss behavior of χ_Q in HTSC, which is reproduced by the FLEX approximation for all compoounds (see Fig. 12).

B. Resistivity and Hall coefficient

In Sec. V, we find that the vertex correction from the MT term gives singular behaviors. In this subsection, we obtain the self-consistent solution for σ_{xx} and σ_{xy}/H, by using the self-consistent Green function given by the FLEX approximation. We solve the BS equation for $J_{\mathbf{k}\mu}(\omega)$ explicitly by including all the MT terms. Here we do not use Eqs. (17), (19), and (22) because the energy integration in deriving them have been done under the assumption that $z_k\Delta_{\mathbf{k}}\ll T$. However, $z_k\Delta_{\mathbf{k}}\sim T$ is realized as shown in the previous subsection. By this reason, we perform the energy integration seriously by taking account of the energy dependence of $v_{\mathbf{k}\mu}(\omega)=v^0_{\mathbf{k}\mu}+d\,{\rm Re}\,\Sigma_{\mathbf{k}}(\omega)/dk_\mu$, $\Delta_{\mathbf{k}}(\omega)=-{\rm Im}\,\Sigma_{\mathbf{k}}(\omega+{\rm i}\delta)$, $V_k(\omega)$, and $J_{\mathbf{k}\mu}(\omega)$ for the numerical calculations of the transport properties.

To obtain σ_{xx} and σ_{xy}/H, we solve the following equations self-consistently:

$$\sigma_{xx}=e^2\sum_{\mathbf{k}}\int\frac{d\epsilon}{\pi}\left(-\frac{\partial f}{\partial\epsilon}\right)\left(|G_{\mathbf{k}}(\epsilon)|^2 v_{\mathbf{k}x}(\epsilon)J_{\mathbf{k}x}(\epsilon)-{\rm Re}\{G^2_{\mathbf{k}}(\epsilon)v^2_{\mathbf{k}x}(\epsilon)\}\right), \tag{49}$$

$$\sigma_{xy}/H=-e^3\sum_{\mathbf{k}}\int\frac{d\epsilon}{2\pi}\left(-\frac{\partial f}{\partial\epsilon}\right)\times|{\rm Im}G_{\mathbf{k}}(\epsilon)||G_{\mathbf{k}}(\epsilon)|^2A_s(\mathbf{k},\epsilon), \tag{50}$$

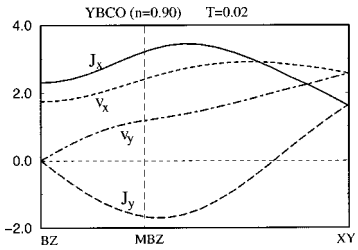

FIG. 16. The obtained $\vec{J}(k_\parallel)$ together with $\vec{v}(k_\parallel)$ on the FS.

$$A_s(\mathbf{k},\epsilon)=v_{\mathbf{k}x}(\epsilon)\left[J_{\mathbf{k}x}(\epsilon)\frac{\partial}{\partial k_y}J_{\mathbf{k}y}(\epsilon)-J_{\mathbf{k}y}(\epsilon)\frac{\partial}{\partial k_y}J_{\mathbf{k}x}(\epsilon)\right]+\langle x\leftrightarrow y\rangle, \tag{51}$$

$$J_{\mathbf{k}\mu}(\omega)=v_{\mathbf{k}\mu}(\omega)+\sum_{\mathbf{q}}\int\frac{d\epsilon}{2\pi}\left[{\rm cotanh}\frac{\epsilon-\omega}{2T}-\tanh\frac{\epsilon}{2T}\right]\times{\rm Im}\,V_{\mathbf{k}-\mathbf{q}}(\epsilon-\omega+{\rm i}\delta)|G_{\mathbf{q}}(\epsilon)|^2J_{\mathbf{q}\mu}(\epsilon), \tag{52}$$

where $f(\epsilon)=\{\exp[(\epsilon-\mu)/T]+1\}^{-1}$, and $G(\omega+{\rm i}\delta)$ and $\Sigma(\omega+{\rm i}\delta)$ are derived from $G(\omega_n)$ and $\Sigma(\omega_n)$ through the numerical analytic continuation.[53] We note that $|G_{\mathbf{k}}(\omega)|^2=\pi\rho_{\mathbf{k}}(\omega)/\Delta_{\mathbf{k}}(\omega)$ and $|G_{\mathbf{k}}(\omega)|^2\cdot{\rm Im}\,G_{\mathbf{k}}(\omega)=\pi\rho_{\mathbf{k}}(\omega)/2\Delta^2_{\mathbf{k}}(\omega)$. The ϵ integration in the above equations are not difficult because its leading contribution comes only from $|\epsilon|\lesssim T$. As for the conductivity, the existence of the second term of Eq. (49), whose derivation will be published elsewhere, has been overlooked in the literature so far. It gives a quantitatively important contribution in the case of $z_{\mathbf{k}}\Delta_{\mathbf{k}}\sim T$.

Because $\Sigma_{\mathbf{k}}(\omega)$ satisfies the self-consistency condition, $v_{\mathbf{k}\mu}(\omega)$ includes all the vertex corrections (a)–(c) in Fig. 7 automatically. Whereas $J_{\mathbf{k}}(\omega)$ contains only the (a) process of $\mathcal{T}_{\mathbf{k}\mathbf{k}'}(\epsilon,\epsilon')$ in the present calculation because the others give only tiny corrections as shown in Sec. IV and in Appendix B. In this sense, our theory satisfies the condition of the conserving approximation well numerically. We did not find any difficulty in solving the BS equation (52) for $J_{\mathbf{k}\mu}(\omega)$ numerically, since the self-consistency condition for $G_{\mathbf{k}}(\omega)$ is satisfied in the FLEX approximation.[25,26] Figure 16 shows the obtained $\vec{J}(k_\parallel)$ for YBCO on the FS along the path shown in Fig. 14. Its feature is close to the schematic one in Fig. 9. We note that $J_y(k_\parallel)$ is negative around the hot spots in this figure. Clearly, such a region is enlarged in the case of NCCO.

Below, we examine the obtained numerical results for YBCO, NCCO, and LSCO. The calculated temperature dependence of $\rho=1/\sigma_{xx}$ and $R_{\rm H}=(\sigma_{xy}/H)\rho^2$ are shown in Figs. 17 and 18, respectively. In these figures, we also plot the $\rho^0=1/\sigma^0_{xx}$ and $R^0_H=(\sigma^0_{xy}/H)(\rho^0)^2$, where σ^0_{xx} and σ^0_{xy} is given by replacing $J_{\mathbf{k}\mu}(\omega)$ with $v_{\mathbf{k}\mu}(\omega)$ in Eqs. (49) and (50). Both σ^0_{xx} and σ^0_{xy} are equal to those derived by the relaxation time approximation in the Boltzmann transport theory, where the conservation laws are violated.

Resistivity. At first, we discuss the T dependences of the resistivity shown in Fig. 17, where we put $e^2/\hbar=1$. $T=0.1$ corresponds to $\sim$500 K if we assume $|t_0|\sim0.5$ eV. In every case both ρ^0 and ρ show approximate T-linear behaviors,

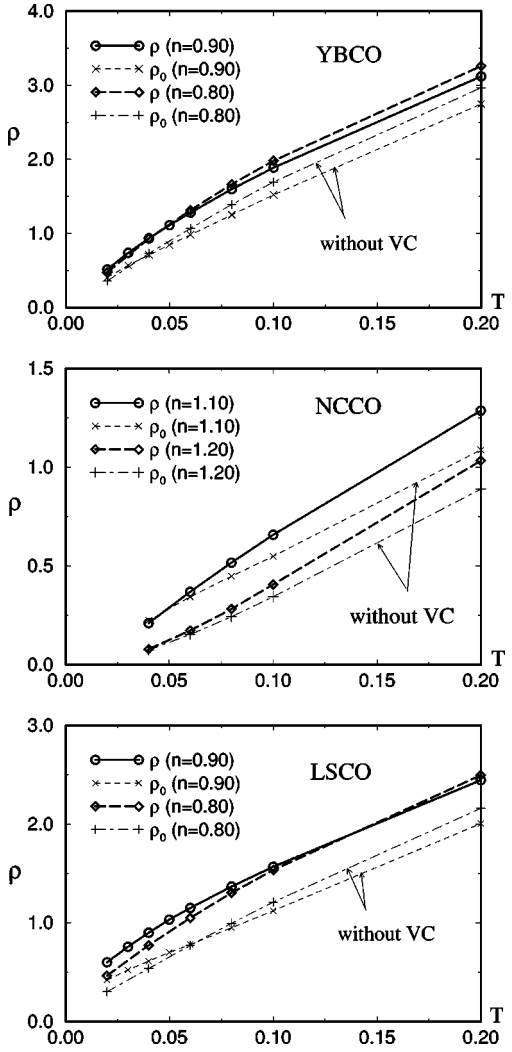

FIG. 17. Temperature dependence of ρ and ρ^0. We find $\rho > \rho^0$ in all the cases. Note that $\rho = 1.0$ in this figure corresponds to $\sim 4 \times 10^{-4}$ Ω cm in single layer compounds. ''VC'' means the vertex corrections for the current. We stress that $d\rho/dT$ increases below $T \approx 0.08$ for YBCO and LSCO, which is caused by the VC, not by the psendo-gap-formation in the DOS.

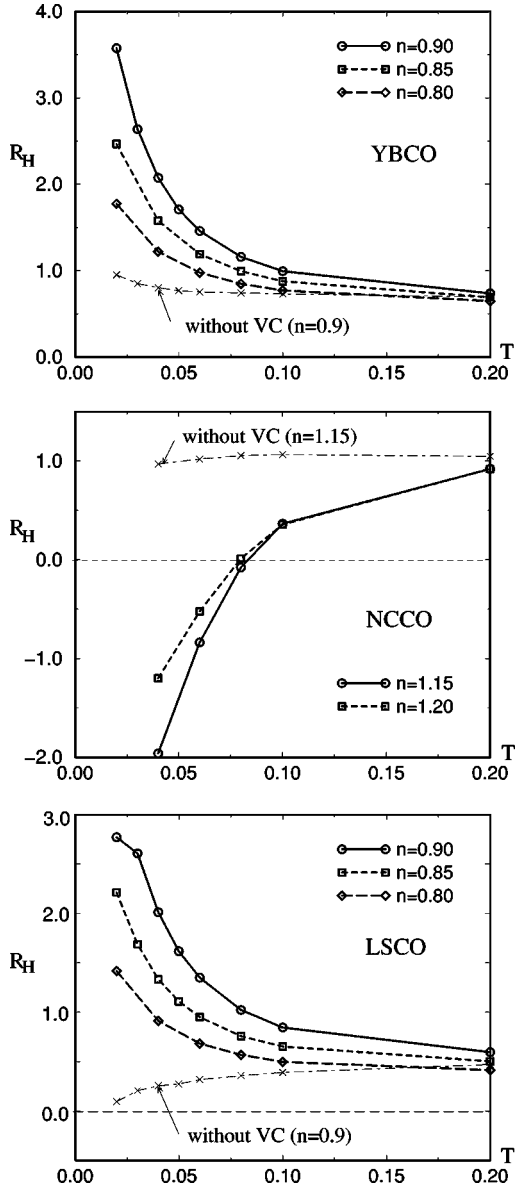

FIG. 18. Temperature dependence of R_H and R_H^0. R_H^0 is denoted by ''without VC''. We see that R_H (more precisely $R_H - R_H^0$) follows the Curie-Weiss type law in all the cases. This universal behavior is ascribed to the T dependence of ξ^2. Here we put $e = 1$. Note that $1/|ne| \sim 1.5 \times 10^{-3}$ cm^3/C in HTSC's.

reflecting the temperature dependence of $\Delta_{\mathbf{k}}$ at the cold spots as shown in Fig. 13.[23,24] They are consistent with experiments. In all the cases the relation $\rho > \rho^0$ is realized, as is expected from the analysis in Sec. V. In LSCO and YBCO, the extrapolated value of ρ^0 at $T = 0$ from the higher temperature region is zero, while that of ρ seems to take a finite value even in a pure system. This behavior of ρ can be explained by looking at Eq. (40) because $\alpha_{\mathbf{k}}$ decreases as T increases, reflecting the decrease of the backward scattering processes at higher temperatures.

The doping dependence of ρ in YBCO and LSCO is very small for $0.8 \leqslant n \leqslant 0.9$ by using the present set of parameters. This behavior is expected qualitatively by Eq. (34), which shows $\langle \Delta_{\mathbf{k}} \rangle_{\mathrm{FS}}$ is independent of ξ in the case of $\omega_{\mathrm{sf}} \lesssim T$. Experimentally, however, $d\rho/dT$ in $La_{2-\delta}Sr_{\delta}CuO_4$ increases for $\delta \geqslant 0.10$ moderately as δ decreases. In this compound, $d\rho_a/dT \approx 1.3 \times 10^{-6}$ [Ω cm] for $\delta = 0.18$ and 2.0×10^{-6} [Ω cm] for $\delta = 0.11$ between $T = 100 \sim 300$ K approximately.[54] This discrepancy will be improved by choosing the more appropriate set of parameters. Apparently, we cannot reproduce the doping dependence of the residual resistivity observed experimentally because we neglect the impurity effect.

Hall Coefficient. Next, we discuss R_H shown in Fig. 18. At higher temperatures $T \sim 0.2$, where $\xi \ll 1$ is satisfied, we see that $R_H \approx R_H^0$ for all compounds. In all cases, $|R_H - R_H^0|$ increases following the Curie-Weiss like behavior as T decreases. Moreover, its coefficient increases rapidly as the filling approaches to $n = 1$, which is consistent with the experimental relation $R_H \propto |1-n|^{-1}$. These behaviors are consistent with the analysis in Sec. V.

Moreover, the sign of R_H in NCCO changes to negative below $T \approx 0.08|t_0| \sim 400$ K, which is consistent with experiments. The Boltzmann approximation cannot explain this behavior because the shape of the FS is holelike everywhere. In

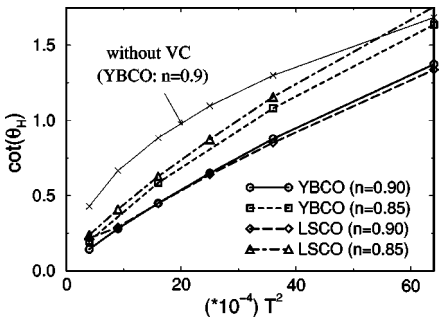

FIG. 19. T dependence of the Hall angle as $\cot(\theta_H)$ vs T^2 in YBCO and LSCO, for $0.02 \leqslant T \leqslant 0.08$. The thin line represents the $\cot(\theta_H^0)$ obtained within the Boltzmann approximation.

the case of LSCO, the FS around $(\pm\pi,0)$ or $(0,\pm\pi)$ are convex in the overdoped region. In this case R_H^0 can be negative within the Boltzmann approximation. Experimentally, R_H in $La_{1-x}Sr_xCuO_2$ becomes negative and almost temperature independent for $x \gtrsim 0.32$, where no superconducting transition occurs and the AF fluctuations are very weak. In the present calculation for LSCO at $n=0.65$, we find that R_H is nearly zero for $T=0.2-0.02$, and $R_H \approx R_H^0$ is realized. As a result, important features of R_H in LSCO are reproduced in the present study for $|1-n| \geqslant 0.1$.

Here, we consider the T dependence of the Hall coefficient given by the Boltzmann approximation. First, we consider the effect of the T dependence of the shape of the FS. As shown in Fig. 10, the curvature of the FS around the cold spots decreases as T decreases, which should make $|R_H^0|$ smaller. Secondly, we discuss the T dependence of $r = \Delta_{\rm cold}/\Delta_{\rm hot}$, which becomes smaller at low temperatures as shown in Fig. 15. This effect makes $|R_H^0|$ larger at low T because only the cold electrons contribute to the transport phenomena then. This mechanism has been pointed out by several authors to explain the enhancement of R_H^0 in YBCO.[23,24] For this reason, R_H^0 of YBCO slightly increases at $T<0.05$ in Fig. 18, where $r \propto \sqrt{T}$ is observed. However, R_H^0 decreases moderately in LSCO, which means that the effect of the change of the FS is stronger. In conclusion, through the cancellation of these two effects, the Hall coefficient given by the Boltzmann transport approximation is nearly $1/ne$ and is not enhanced significantly.

Now we stress that R_H in our calculation follows the Curie-Weiss law, even if the T dependence of the FS is taken into account. Undoubtedly, this behavior of R_H comes from the vertex corrections for the current, which is proportional to χ_Q as shown in Eq. (44). In fact, the calculated R_H are similar to those of χ_Q shown in Fig. 12, in all cases. In summary, the vertex corrections for the current are essential for the Curie-Weiss behavior of R_H in HTSC's observed experimentally. This universal behavior of R_H is quite robust in the present calculations.

Hall Angle. We also discuss the temperature dependence of the Hall angle θ_H, which is defined by $\cot(\theta_H) = \sigma_{xx}/(\sigma_{xy}/H) = \rho/R_H$. Figure 19 shows that $\cot(\theta_H)$ is approximately proportional to T^2 for $0.02 \leqslant T \leqslant 0.08$. This relation has been observed experimentally in various kinds of HTSC's for $T=100-300$ K.[5,7,8] Our theory can explain this relation without assuming the non-Fermi-liquid ground state

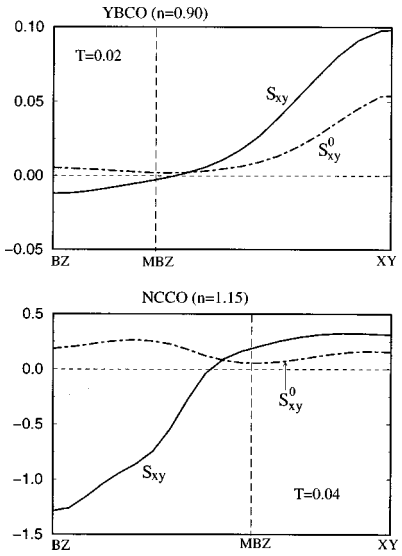

FIG. 20. $k_\parallel$ dependence of $S_{xy}(k_\parallel)$ and $S_{xy}^0(k_\parallel)$ on the FS (see Fig. 14).

which possesses two kinds of relaxation rates.[55] Figure 19 means that R_H follows the Curie-Weiss behavior, because ρ is proportional to T. We stress that the relation $\cot(\theta_H) \propto T^2$ is also observed experimentally in κ-BEDT-TTF compounds[67] or in V_2O_3,[70] both of them are also nearly AF Fermi liquids.

Here, we discuss the following functions:

$$S_{xy}(k_\parallel) \equiv -\int dk_\perp \rho_{\mathbf{k}}(0) A_s(\mathbf{k},0) \frac{1}{(\Delta_{\mathbf{k}}(0))^2}$$

$$= -|\vec{J}(k_\parallel)|^2 \left(\frac{d\theta_J(k_\parallel)}{dk_\parallel} \right) \frac{1}{\{\Delta(k_\parallel)\}^2}, \qquad (53)$$

where $k_\parallel$ is the momentum along the FS. $A_s(\mathbf{k},\epsilon)$ is given by Eq. (51), and $k_\perp$ is the momentum perpendicular to the FS. It is clear that $\sigma_{xy}/H = \int_{\rm FS} dk_\parallel S_{xy}(k_\parallel)$. We also define $S_{xy}^0(k_\parallel)$ by replacing $J_{\mathbf{k}\mu}$ with $v_{\mathbf{k}\mu}$ in Eq. (52), which means that $\sigma_{xy}^0/H = \int_{\rm FS} dk_\parallel S_{xy}^0(k_\parallel)$. Figure 20 shows the $k_\parallel$ dependence of $S_{xy}(k_\parallel)$ and $S_{xy}^0(k_\parallel)$ along the path shown in Fig. 14. In both cases of YBCO and NCCO, $S_{xy}^0(k_\parallel)$ is positive everywhere. Whereas, $S_{xy}(k_\parallel)$ is positive inside the MBZ and negative outside of it, which is consistent with the analysis in Sec. V.

In the case of YBCO, $S_{xy}(k_\parallel)$ takes a maximum value on the XY axis because it is a cold spot for YBCO. It takes an enhanced value because the relation $S_{xy}(k_{\rm cold})/S_{xy}^0(k_{\rm cold}) = 1/[1-\alpha^2(k_{\rm cold})] \propto \xi^2$ is expected according to Eq. (43). As a result, $R_H \propto \xi^2$ is realized. We have also calculated $S_{xy}(k_\parallel)$ for LSCO, and found that its behavior is similar to that for YBCO in spite of the incommensurability of $\chi(q,0)$.

On the other hand, in the case of NCCO, $S_{xy}(k_\parallel)$ takes a maximum value on the BZ boundary which is a cold spot of NCCO. It is also enhanced because $S_{xy}(k_{\rm cold})/S_{xy}^0(k_{\rm cold}) \propto \beta_\parallel(k_{\rm cold}) \propto \xi^2$ is expected by Eq. (43) in this case. As a result, $R_H \propto -\xi^2$ is realized and it becomes negative at low temperatures.

VII. SUMMARY AND DISCUSSIONS

First, we outline the main results of this paper. We have calculated the conductivity σ_{xx} and the Hall conductivity σ_{xy}/H in the single-band Hubbard model based on the Fermi-liquid theory. We have calculated the total current $\vec{J}_{\mathbf{k}}$ including the vertex corrections, which are demanded in the framework of the conservation approximation by Baym and Kadanoff. In nearly AF Fermi liquids, the Bethe-Salpeter Eq. (19) for $\vec{J}_{\mathbf{k}}$ can be simplified to Eq. (38), which is solved easily. The obtained $\vec{J}_{\mathbf{k}}$ shows nontrivial critical behaviors as seen in Fig. 9, which is the natural consequence of the strong backward scatterings caused by the strong AF fluctuations. In conclusion, $R_H \propto \xi^2$ is realized in HTSC's through the anomaly of $\vec{J}_{\mathbf{k}}$. This mechanism has not been pointed out previously.

We also have done the numerical calculations by using the FLEX approximation. We can reproduce characteristic features of the spin fluctuations for YBCO, NCCO, and LSCO, by using the appropriate set of parameters. In each case, $d_{x^2-y^2}$ superconductivity is realized at $T_c = 50-100$ K. Next, we have determined $\vec{J}_{\mathbf{k}}$ by solving Eq. (19) numerically, and calculated both ρ and R_H for various filling numbers. As shown in Fig. 18, the overall features of R_H in each compound are reproduced quite well. Especially, both the relations $R_H \propto 1/T$ and $\rho \propto T$ are obtained at the same time. We have found that $R_H < 0$ is realized in NCCO because the cold spots in NCCO locate around the BZ boundaries, which may be verified by ARPES experiments.

The vertex corrections mentioned above are not included in the Boltzmann approximation. We have confirmed that the Hall coefficient given by the Boltzmann approximation R_H^0 remains of order $O(1/ne)$ if we take the T dependence of the interacting FS into account correctly (see Fig. 18). Moreover, R_H^0 remains positive because the FS is holelike everywhere. In conclusion, the anomalous behaviors of R_H in HTSC is reproducible only if the vertex corrections for the current are taken into account.

Here, we discuss the validity of the relation $R_H \propto \xi^2$ given by Eq. (44). In a conserving approximation (including the FLEX approximation) the interaction $V_{\mathbf{k}}(\omega)$ which gives $\mathrm{Im}\,\Sigma_{\mathbf{k}}(\omega)$ also determines the MT-type vertex corrections for $\vec{J}_{\mathbf{k}}$, as shown by Eqs. (32) and (36). This condition leads to $\alpha_{\mathbf{k}} \sim 1$ in Eq. (38), which strongly suggests that $R_H \propto \xi^2$ will be valid beyond the FLEX approximation. Now we assume that the relation $R_H \propto \xi^2$ is valid near the half filling case ($n \approx 1$). Then, the experimental relation $\max\{|R_H|\} \propto |1-n|^{-1}$ is derived qualitatively because $\max\{\xi^2\} \propto |1-n|^{-1}$ is observed experimentally near half filling. Next, we consider the Hall coefficient below T^*, where R_H in YBCO decreases as T decreases experimentally. It is also consistent with the theoretical relation $R_H \propto \xi^2$ because ξ slightly decreases below T^* experimentally.[56]

Unfortunately, the FLEX approximation becomes insufficient near the Mott insulating state. By this reason, we did not apply the present method for $0.9 \leqslant n \leqslant 1.1$. Experimentally, both $|R_H|$ and $d\rho/dT$ for $0.9 \leqslant n \leqslant 1.1$ increases rapidly as $n \to 1$. The FLEX approximation is also inappropriate for study of the electronic states below T^*, which is one of the important future problems on HTSC. Recently, Ref. 57 calculated some vertex parts of the self-energy. As an alternative possibility, the preformed pairs may be formed for $T < T^*$. This scenario has been intensively studied recently.[58,59]

In Ref. 34, it is shown that a similar numerical study based on the AF spin-fluctuation model also leads to the enhancement of R_H, by using the set of spin fluctuation parameters consistent with experiments. Although the conservation laws are not satisfied exactly in that study, it confirms the importance of the vertex corrections for the current. It indicates that the numerical results presented in this paper should not be taken as an artifact specific to the FLEX approximation.

Now we would like to discuss R_{H} in heavy Fermion (HF) compounds. In the paramagnetic compounds, R_H shows a drastic temperature dependence and takes an enhanced value.[60–62] At low temperatures, the relation $R_H = c\rho^2$ is observed in many compounds, and the coefficient c is positive for all compounds. It is explained in terms of the anomalous Hall effect (AHE), which originates from the localized f-orbital angular momentum, and its enhancement factor is given by $\chi_0 \equiv \chi_{\mathbf{q}=0}(0)$.[63,64] On the other hand, in many HF compounds with AF ground state, the relation $R_H = c\rho^2$ is not satisfied and the sign of dR_H/dT at $T > T_N$ changes depending on compounds.[60–62] This behavior is also observed in non-Fermi-liquid HF compounds, which is near the AF quantum phase boundary, e.g., $Ce(Ni_{1-x}Pd_x)_2Ge_2$.[65] We stress that the normal Hall effect can exceed the AHE and $R_H \propto X_Q$ will be realized in these nearly antiferromagnetic HF compounds, where $\chi_Q \gg \chi_0$ is realized. We note that $\chi_Q \propto (T-T_{\mathrm{N}})^{-3/2}$ in three dimensions is obtained by the SCR theory.

We also comment on the κ-BEDT-TTF organic superconductors. Several experiments show that R_H of this system increases as T decreases.[66,67] This will be explained according to our theory, because the recent studies based on the FLEX calculation reveal that there are large AF fluctuations in κ-BEDT-TTF compounds, which are the origin of the d-wave superconductivity.[44,45] Also, the relation $R_H \propto 1/T$ is observed in the superconducting ladder compound $Sr_{14-x}Ca_xCu_{24}O_{41}$.[68] The main electronic properties in this compound, e.g., the pseudogap behavior and the d-wave superconductivity, are well explained by the FLEX approximation.[43] In addition, R_H in V_2O_3 shows the singular T dependence near the AF phase boundary.[69,70]

ACKNOWLEDGMENTS

We are grateful to Kosaku Yamada for stimulating discussions. We also thank T. Moriya, H. Fukuyama, M. Satoh, H. Kohno, and Y. Yanase for valuable comments. This work was financially supported by a Grant-in-Aid for Scientific Research on Priority Areas from the Ministry of Education, Science, Sports and Culture.

APPENDIX A: ANALYTIC CONTINUATION FOR $\Gamma(\epsilon_N, \epsilon_{n'})$

In this appendix, we derive the irreducible vertex $\mathcal{T}_{\mathbf{k}\mathbf{k}'}(\epsilon, \epsilon')$ which are the kernel of the BS equation, Eq. (19). For this purpose, we perform the analytic continuation for

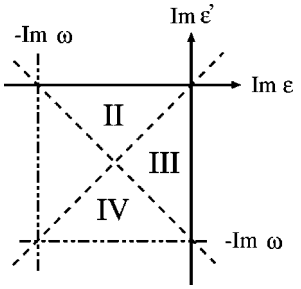

FIG. 21. $\Gamma(\epsilon,\epsilon';\omega)$ ($\omega>0$) is an analytic function inside of each (II,III,IV) region, and has the cuts on each line.

$\Gamma(\epsilon_n,\epsilon_{n'};\omega_l)$, where $\omega_l=2\pi Tl$ ($l>0$) is the external frequency. The irreducible vertices consistent with the FLEX approximation are given by Eqs. (26)–(28).

According to Eq. (12) in Ref. 27,

$$\mathcal{T}_{\mathbf{k}\mathbf{k}'}(\epsilon,\epsilon')=\mathrm{cotanh}\frac{\epsilon'-\epsilon}{2T}[\Gamma^{\mathrm{II}}_{\mathbf{k}\mathbf{k}'}(\epsilon,\epsilon')-\Gamma^{\mathrm{III}}_{\mathbf{k}\mathbf{k}'}(\epsilon,\epsilon')]+\mathrm{cotanh}\frac{\epsilon'+\epsilon}{2T}[\Gamma^{\mathrm{III}}_{\mathbf{k}\mathbf{k}'}(\epsilon,\epsilon')-\Gamma^{\mathrm{IV}}_{\mathbf{k}\mathbf{k}'}(\epsilon,\epsilon')]-\tanh\frac{\epsilon'}{2T}[\Gamma^{\mathrm{II}}_{\mathbf{k}\mathbf{k}'}(\epsilon,\epsilon')-\Gamma^{\mathrm{IV}}_{\mathbf{k}\mathbf{k}'}(\epsilon,\epsilon')],\quad\text{(A1)}$$

where $\Gamma^{\mathrm{II}}(\epsilon,\epsilon')$, $\Gamma^{\mathrm{III}}(\epsilon,\epsilon')$ and $\Gamma^{\mathrm{IV}}(\epsilon,\epsilon')$ are given by the analytic continuations of $\Gamma(\epsilon_n,\epsilon_{n'};\omega_l)$ for regions II, III, and IV in the complex (ϵ,ϵ') plane shown in Fig. 21, respectively.

Next, we take the limit $i\omega\to+0$. For Eq. (26), we get

$$\Gamma^{(a)\mathrm{II}}_{\mathbf{k}\mathbf{k}'}(\epsilon,\epsilon')=V^R(\mathbf{k}-\mathbf{k}',\epsilon'-\epsilon),\quad\text{(A2)}$$

$$\Gamma^{(a)\mathrm{III}}_{\mathbf{k}\mathbf{k}'}(\epsilon,\epsilon')=\Gamma^{(a)\mathrm{IV}}_{\mathbf{k}\mathbf{k}'}(\epsilon,\epsilon')=V^A(\mathbf{k}-\mathbf{k}',\epsilon'-\epsilon),\quad\text{(A3)}$$

where $A(R)$ represents the advanced (retarded) function. Taking account of the relation $\mathrm{Im}\{\epsilon'-\epsilon\}>0$ in the II region and $\mathrm{Im}\{\epsilon'-\epsilon\}<0$ in the III,IV region, we get for Eq. (27) as

$$\Gamma^{(b)\mathrm{II}}_{\mathbf{k}\mathbf{k}'}(\epsilon,\epsilon')=\sum_{\mathbf{q}}\int\frac{d\omega}{2\pi}W_{\mathbf{q}}(\omega)\Big[\tanh\frac{\omega+\epsilon}{2T}\mathrm{Im}\,G^R_{\mathbf{k}+\mathbf{q}}(\omega+\epsilon)\times G^R_{\mathbf{k}'+\mathbf{q}}(\omega+\epsilon')+\tanh\frac{\omega+\epsilon'}{2T}\times G^A_{\mathbf{k}+\mathbf{q}}(\omega+\epsilon)\mathrm{Im}\,G^R_{\mathbf{k}'+\mathbf{q}}(\omega+\epsilon')\Big]+C,\quad\text{(A4)}$$

$$\Gamma^{(b)\mathrm{III}}_{\mathbf{k}\mathbf{k}'}(\epsilon,\epsilon')=\Gamma^{(b)\mathrm{IV}}_{\mathbf{k}\mathbf{k}'}(\epsilon,\epsilon')=\sum_{\mathbf{q}}\int\frac{d\omega}{2\pi}W_{\mathbf{q}}(\omega)\times\Big[\tanh\frac{\omega+\epsilon}{2T}\mathrm{Im}\,G^R_{\mathbf{k}+\mathbf{q}}(\omega+\epsilon)G^A_{\mathbf{k}'+\mathbf{q}}(\omega+\epsilon')+\tanh\frac{\omega+\epsilon'}{2T}G^R_{\mathbf{k}+\mathbf{q}}(\omega+\epsilon)\mathrm{Im}\,G^R_{\mathbf{k}'+\mathbf{q}}(\omega+\epsilon')\Big]+C,\quad\text{(A5)}$$

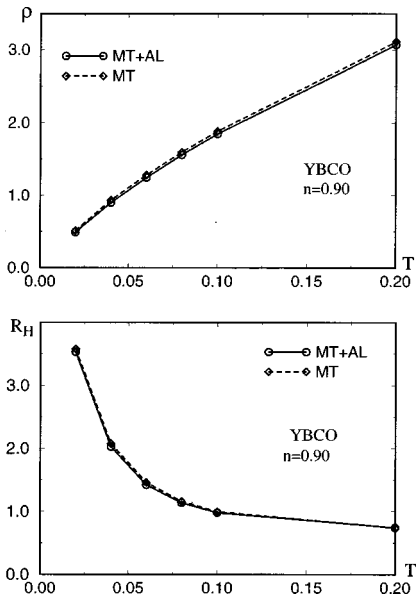

FIG. 22. The obtained T dependence of the resistivity and the Hall coefficient. MT and MT+AL are given by $J_{\mathbf{k}\mu}(\omega)$ derived from Eqs. (52) and (B1), respectively.

where C is a real function, and $W_{\mathbf{q}}(\omega)$ is given by

$$W_{\mathbf{q}}(\omega)=\frac{3}{2}U^2|U\chi^s_{\mathbf{q}}(\omega)+1|^2+\frac{1}{2}U^2|U\chi^c_{\mathbf{q}}(\omega)-1|^2-U^2.\quad\text{(A6)}$$

In the same way, taking the relation $\mathrm{Im}\{\epsilon'+\epsilon+\omega\}>0$ in the II,III region and $\mathrm{Im}\{\epsilon'+\epsilon+\omega\}<0$ in the IV region into account, we get for Eq. (28) as

$$\Gamma^{(c)\mathrm{II}}_{\mathbf{k}\mathbf{k}'}(\epsilon,\epsilon')=\Gamma^{(c)\mathrm{III}}_{\mathbf{k}\mathbf{k}'}(\epsilon,\epsilon')=\sum_{\mathbf{q}}\int\frac{d\omega}{2\pi}W_{\mathbf{q}}(\omega)\times\Big[\tanh\frac{\omega+\epsilon}{2T}\mathrm{Im}\,G^R_{\mathbf{k}+\mathbf{q}}(\omega+\epsilon)G^R_{\mathbf{k}'+\mathbf{q}}(-\omega+\epsilon')+\tanh\frac{\omega-\epsilon'}{2T}G^R_{\mathbf{k}+\mathbf{q}}(\omega+\epsilon)\times\mathrm{Im}\,G^R_{\mathbf{k}'+\mathbf{q}}(-\omega+\epsilon')\Big]+C',\quad\text{(A7)}$$

$$\Gamma^{(c)\mathrm{IV}}_{\mathbf{k}\mathbf{k}'}(\epsilon,\epsilon')=\sum_{\mathbf{q}}\int\frac{d\omega}{2\pi}W_{\mathbf{q}}(\omega)\Big[\tanh\frac{\omega+\epsilon}{2T}\times\mathrm{Im}\,G^R_{\mathbf{k}+\mathbf{q}}(\omega+\epsilon)G^A_{\mathbf{k}'+\mathbf{q}}(-\omega+\epsilon')+\tanh\frac{\omega-\epsilon'}{2T}G^A_{\mathbf{k}+\mathbf{q}}(\omega+\epsilon)\times\mathrm{Im}\,G^R_{\mathbf{k}'+\mathbf{q}}(-\omega+\epsilon')\Big]+C',\quad\text{(A8)}$$

where C' is a real function.

By inserting the above equations into Eq. (A1), $\mathcal{T}_{\mathbf{k},\mathbf{k}'}(\epsilon_n,\epsilon_{n'};\omega_l)$ is given by $\mathcal{T}^{(a)}+\mathcal{T}^{(b)}+\mathcal{T}^{(c)}$. They are derived as

$$\mathcal{T}^{(a)}_{\mathbf{k},\mathbf{k}'}(\epsilon,\epsilon')=\left(\mathrm{cotanh}\frac{\epsilon'-\epsilon}{2T}-\tanh\frac{\epsilon'}{2T}\right)\times 2i\,\mathrm{Im}\,V_{\mathbf{k}'-\mathbf{k}}(\epsilon'-\epsilon+i\delta), \tag{A9}$$

$$\mathcal{T}^{(b)}_{\mathbf{k},\mathbf{k}'}(\epsilon,\epsilon')=\left(\mathrm{cotanh}\frac{\epsilon'-\epsilon}{2T}-\tanh\frac{\epsilon'}{2T}\right)\sum_{\mathbf{q}}\int d\omega\, W_{\mathbf{q}}(\omega)\times(-i\pi)\left(\tanh\frac{\omega+\epsilon}{2T}-\tanh\frac{\omega+\epsilon'}{2T}\right)\times\rho_{\mathbf{k}+\mathbf{q}}(\omega+\epsilon)\rho_{\mathbf{k}'+\mathbf{q}}(\omega+\epsilon'), \tag{A10}$$

$$\mathcal{T}^{(c)}_{\mathbf{k},\mathbf{k}'}(\epsilon,\epsilon')=\left(\mathrm{cotanh}\frac{\epsilon'+\epsilon}{2T}-\tanh\frac{\epsilon'}{2T}\right)\sum_{\mathbf{q}}\int d\omega\, W_{\mathbf{q}}(\omega)\times(-i\pi)\left(\tanh\frac{\omega+\epsilon}{2T}+\tanh\frac{\omega-\epsilon'}{2T}\right)\times\rho_{\mathbf{k}+\mathbf{q}}(\omega+\epsilon)\rho_{\mathbf{k}'-\mathbf{q}}(-\omega+\epsilon'). \tag{A11}$$

Note that $\mathcal{T}^{(a-c)}_{\mathbf{k}\mathbf{k}'}(\epsilon,\epsilon')$ is purely imaginary.

APPENDIX B: CORRECTIONS FROM THE AL TERMS FOR $J_{\mathbf{k}\mu}$

In this appendix, we study the contributions from the AL terms to the total current $\vec{J}_{\mathbf{k}}$. For this purpose, we solve the BS equation for $\vec{J}_{\mathbf{k}}(\omega)$ including both the MT process and AL processes, and compare the obtained results with those in Sec. VI B. The exact Bethe-Salpeter equation is

$$J_{\mathbf{k}\mu}(\omega)=v_{\mathbf{k}\mu}(\omega)+\sum_{r}^{a,b,c}\Delta J^{r}_{\mathbf{k}\mu}(\omega), \tag{B1}$$

$$\Delta J^{r}_{\mathbf{k}\mu}(\omega)=\sum_{\mathbf{q}}\int_{-\infty}^{\infty}\frac{d\epsilon}{4i}\mathcal{T}^{(r)}_{\mathbf{k},\mathbf{q}}(\omega,\epsilon)\frac{\rho_{\mathbf{q}}(\epsilon)}{\Delta_{\mathbf{q}}(\epsilon)}J_{\mathbf{q}\mu}(\epsilon), \tag{B2}$$

where $r=a,b,c$ and $\mathcal{T}^{(r)}_{\mathbf{k},\mathbf{q}}(\omega,\epsilon)$ are given by Eqs. (A9)–(A11). Note that $\mathcal{T}^{(r)}_{\mathbf{k},\mathbf{q}}(\omega,\epsilon)$ are purely imaginary.

For simplicity of the numerical calculation, we put all the energy variables in $\rho_{\mathbf{k}'}(\omega)$, $\Delta_{\mathbf{k}}(\omega)$ and $J_{\mathbf{k}\mu}(\omega)$ as zero for $\Delta J^{b}_{\mathbf{k}\mu}(\omega)$ and $\Delta J^{c}_{\mathbf{k}\mu}(\omega)$. The strict justification of this simplification is difficult, although it may be sufficient for a rough estimation of the magnitude of the AL terms. We represent the solution of Eq. (B1) as $J^{\mathrm{MT+AL}}_{\mathbf{k}\mu}(\omega)$.

Figure 22 shows the resistivity and the Hall coefficient $R_H^{\mathrm{MT+AL}}$ for YBCO ($n=0.90$) derived from $J^{\mathrm{MT+AL}}_{\mathbf{k}\mu}(\omega)$, together with those given in Sec. VI B. We see that the AL terms give only a small correction to ρ and R_H.

[1] See, e.g., Y. Iye, in *Physical Properties of High Temperature Superconductors*, edited by D.M. Ginsberg (World Scientific, Singapore, 1992), Vol. 3.

[2] See, e.g., K. Asayama, Y. Kitaoka, G.-q. Zheng, and K. Ishida, Prog. Nucl. Magn. Reson. Spectrosc. **28**, 221 (1996).

[3] P.B. Allen, W.E. Pickett, and H. Krakauer, Phys. Rev. B **36**, 3926 (1987).

[4] J. Takeda, T. Nishikawa, and M. Sato, Physica C **231**, 293 (1994).

[5] H.Y. Hwang, B. Batlogg, H. Takagi, H.L. Kao, J. Kwo, R.J. Cava, J.J. Krajewski, and W.F. Peck, Jr., Phys. Rev. Lett. **72**, 2636 (1994).

[6] T. Nishikawa, J. Takeda, and M. Sato, J. Phys. Soc. Jpn. **63**, 1441 (1994).

[7] Peng Xiong, Gang Xiao, and X.D. Wu, Phys. Rev. B **47**, 5516 (1993).

[8] T.R. Chien, Z.Z. Wang, and N.P. Ong, Phys. Rev. Lett. **67**, 2088 (1991).

[9] Y. Kubo, Y. Shimakawa, T. Manako, and H. Igarashi, Phys. Rev. B **43**, 7875 (1991).

[10] S. Uchida, H. Takagi, and Y. Tokura, Physica C **162-164**, 1676 (1989).

[11] P. Fournier, X. Jiang, W. Jiang, S.N. Mao, T. Venkatesan, C.J. Lobb, and R.L. Greene, Phys. Rev. B **56**, 14 149 (1997).

[12] T. Moriya, Y. Takahashi, and K. Ueda, J. Phys. Soc. Jpn. **59**, 2905 (1990); K. Ueda, T. Moriya, and Y. Takahashi, J. Phys. Chem. Solids **53**, 1515 (1992).

[13] P. Monthoux and D. Pines, Phys. Rev. B **47**, 6069 (1993).

[14] N.E. Bickers and S.R. White, Phys. Rev. B **43**, 8044 (1991).

[15] P. Monthoux and D.J. Scalapino, Phys. Rev. Lett. **72**, 1874 (1994).

[16] M. Langer, J. Schmalian, S. Grabowski, and K.H. Bennemann, Phys. Rev. Lett. **75**, 4508 (1995).

[17] J.J. Deisz, D.W. Hess, and J.W. Serene, Phys. Rev. Lett. **76**, 1312 (1996).

[18] T. Dahm and L. Tewordt, Phys. Rev. B **52**, 1297 (1995).

[19] D.K. Morr and D. Pines, Phys. Rev. Lett. **81**, 1086 (1998).

[20] T. Takimoto and T. Moriya, J. Phys. Soc. Jpn. **67**, 3570 (1994).

[21] K. Miyake and O. Narikiyo, J. Phys. Soc. Jpn. **63**, 3821 (1994); Physica C **235-240**, 2237 (1994).

[22] F.F. Assaad and M. Imada, Phys. Rev. Lett. **74**, 3868 (1995).

[23] B.P. Stojković and D. Pines, Phys. Rev. B **55**, 8576 (1997). Here, the term $(\omega_{kk'}+\pi T)$ in Eq. (16) should be replaced by $(\omega_{kk'}+\pi T/2)$, as shown in Eq. (32) in the present paper.

[24] Y. Yanase and K. Yamada, J. Phys. Soc. Jpn. **68**, 548 (1999).

[25] G. Baym and L.P. Kadanoff, Phys. Rev. **124**, 287 (1961).

[26] G. Baym, Phys. Rev. **127**, 1391 (1962).

[27] G.M. Eliashberg, Sov. Phys. JETP **14**, 886 (1962).

[28] K. Yamada and K. Yosida, Prog. Theor. Phys. **76**, 621 (1986).

[29] H. Kohno and K. Yamada, Prog. Theor. Phys. **80**, 623 (1988).

[30] H. Fukuyama, H. Ebisawa, and Y. Wada, Prog. Theor. Phys. **42**, 494 (1969).

[31] V. Barzykin and D. Pines, Phys. Rev. B **52**, 13 585 (1995).

[32] The ARPES and STM experiments show that the pseudogap appears in the density of states below T^{**} ($>T^{*}$). Experimentally, $\omega_{\mathrm{sf}}\cdot\xi$ is almost constant and $\xi\propto 1/T$ for $T^{**}>T>T^{*}$. However, the crossover phenomena at $T=T^{**}$ are rather moderate and obscure.

[33] H. Kohno and K. Yamada, Prog. Theor. Phys. **85**, 13 (1991).

[34] K. Kanki and H. Kontani, J. Phys. Soc. Jpn. (to be published).

[35] J. Yu, S. Massidda, A.J. Freeman, and D.D. Koelling, Phys. Lett. A **122**, 203 (1987).

[36] S. Massidda, N. Hamada, J. Yu, and A.J. Freeman, Physica C **157**, 571 (1989).
[37] A.J. Freeman and J. Yu, Physica B **150**, 50 (1988).
[38] J.-H. Xu, T.J. Watson-Yang, J. Yu, and A.J. Freeman, Phys. Lett. A **120**, 489 (1987).
[39] T. Tanamoto, H. Kohno, and H. Fukuyama, J. Phys. Soc. Jpn. **61**, 1886 (1992). We use the same hopping-parameters of YBCO, $(t_1/t_0, t_2/t_0)$, as those in their paper.
[40] J.C. Campuzano, G. Jennings, M. Faiz, L. Beaulaigue, B.W. Veal, J.Z. Liu, A.P. Paulikas, K. Vandervoort, H. Claus, R.S. List, A.J. Arko, and R.J. Bartlett, Phys. Rev. Lett. **64**, 2308 (1990).
[41] D.M. King, Z.-X. Shen, D.S. Dessau, D.S. Marshall, C.H. Park, W.E. Spicer, J.L. Peng, Z.Y. Li, and R.L. Greene, Phys. Rev. Lett. **73**, 3298 (1994).
[42] D.S. Dessau, Z.-X. Shen, D.M. King, D.S. Marshall, L.W. Lombardo, P.H. Dickinson, A.G. Loeser, J. DiCarlo, C.-H. Park, A. Kapitulnik, and W.E. Spicer, Phys. Rev. Lett. **71**, 2781 (1993).
[43] H. Kontani and K. Ueda, Phys. Rev. Lett. **80**, 5619 (1998).
[44] H. Kino and H. Kontani, J. Phys. Soc. Jpn. **67**, 3691 (1998).
[45] H. Kondo and T. Moriya, J. Phys. Soc. Jpn. **67**, 3695 (1998).
[46] M. Tsuji, J. Phys. Soc. Jpn. **13**, 979 (1958).
[47] J.M. Zimann, *Electrons and Phonons* (Clarendon, Oxford, 1960).
[48] N.P. Ong, Phys. Rev. B **43**, 193 (1991).
[49] S. Koikegami, S. Fujimoto, and K. Yamada, J. Phys. Soc. Jpn. **66**, 1438 (1997).
[50] Henry Chou, J.M. Tranquada, G. Shirane, T.E. Mason, W.J.L. Buyers, S. Shamoto, and M. Sato, Phys. Rev. B **43**, 5554 (1991).
[51] M. Matsuda, K. Yamada, Y. Endoh, T.R. Thurston, G. Shirane, R.J. Birgeneau, M.A. Kastner, I. Tanaka, and H. Kojima, Phys. Rev. B **49**, 6958 (1994).
[52] H. Ding, M.R. Norman, T. Yokoya, T. Takeuchi, M. Randeria, J.C. Campuzano, T. Takahashi, T. Mochiku, and K. Kadowaki, Phys. Rev. Lett. **78**, 2628 (1997).
[53] H.J. Vidberg and J.W. Serene, J. Low Temp. Phys. **19**, 179 (1977).
[54] T. Kimura, S. Miyasaka, H. Takagi, K. Tamasaku, H. Eisaki, S. Uchida, K. Kisazawa, M. Hiroi, M. Sera, and N. Kobayashi, Phys. Rev. B **53**, 8733 (1996).
[55] P.W. Anderson, Phys. Rev. Lett. **67**, 2092 (1991).
[56] Y. Itoh, T. Magchi, S. Adachi, A. Fukuoka, K. Tanabe, and H. Yasuoka, J. Phys. Soc. Jpn. **67**, 312 (1998).
[57] J. Schmalian, D. Pines, and B. Stojković, Phys. Rev. Lett. **80**, 3839 (1998).
[58] S. Koikegami and K. Yamada, J. Phys. Soc. Jpn. **67**, 1114 (1998).
[59] T. Dahm, D. Manske, and L. Tewordt, Phys. Rev. B **55**, 15 274 (1997).
[60] Y. Ōnuki, T. Yamayoshi, I. Ukon, T. Komatsubara, A. Umezawa, W.K. Kwok, G.W. Crabtree, and D.G. Hinks, J. Phys. Soc. Jpn. **58**, 2119 (1989).
[61] Y. Ōnuki, T. Yamayoshi, T. Omi, I. Ukon, A. Kobori, and T. Komatsubara, J. Phys. Soc. Jpn. **58**, 2126 (1989).
[62] Y. Ōnuki, S.W. Yun, K. Satoh, H. Sugawara, and H. Sato, in *Transport and Thermal Property of f-electron Systems*, edited by Oomi *et al.* (Plenum Press, New York, 1993), p 103.
[63] H. Kontani and K. Yamada, J. Phys. Soc. Jpn. **63**, 2627 (1994): In the multiband system due to the orbital degeneracy, the anomalous Hall effect (AHE) can exist in principle. The AHE causes the drastic temperature $R_H \propto \rho^2$ at low temperatures. It is highly enhanced due to the correlation effect in heavy Fermion compounds.
[64] H. Kontani, M. Miyazawa, and K. Yamada, J. Phys. Soc. Jpn. **66**, 2252 (1997).
[65] T. Fukuhara, S. Akamaru, T. Kuwai, J. Sakurai, and K. Maezawa, J. Phys. Soc. Jpn. **67**, 2084 (1998).
[66] K. Murata, M. Ishibashi, Y. Honda, N.A. Fortune, M. Tokumoto, N. Kinoshita, and H. Anzai, Solid State Commun. **76**, 377 (1990).
[67] Yu. V. Sushko, N. Shirakawa, K. Murata, Y. Kubo, N.D. Kushch, and E.B. Yagubskii, Synth. Met. **85**, 1541 (1997).
[68] T. Nakanishi, N. Môri, C. Murayama, H. Takahashi, T. Nagata, M. Uehara, J. Akimitsu, K. Kinoshita, N. Motoyama, H. Eisaki, and S. Uchida, J. Phys. Soc. Jpn. **67**, 2408 (1998).
[69] S. Klimm, G. Gerstmeier, H. Paulin, M. Klemm, and S. Horn, Physica B **230-232**, 992 (1997).
[70] T.F. Rosenbaum, A. Husmann, S.A. Carter, and J.M. Honig, Phys. Rev. B **57**, R13 997 (1998).